X-RAY FOCUSING OPTICS

by

Patrick Thrasher

A Thesis Submitted to the Faculty of the

COLLEGE OF OPTICAL SCIENCES

In Partial Fulfillment of the Requirements

For the Degree of

MASTER OF SCIENCE

In the Graduate College

THE UNIVERSITY OF ARIZONA

2016

Contents

List of Figures

Abstract

The existence of x-rays has only been known for the last 150 years. Compared this to visible optics, which have been studied in earnest for almost a millennium, the study of x-rays is still in its infancy. While many of the properties of x-rays are well known, they are not particularly easy to work with, making the optical designs to focus them much more complicated. As the energy of x-rays increases, they become more difficult to handle, to the point where they become gamma rays which cannot be focused at all. Because of the need for such specialized focusing optics, there is not much of a commercial market for their use, although there have been numerous x-ray telescopes that have been launched by various national space agencies to study both the sun and distant galaxies. The design of the majority of these telescopes has not changed much since their inception in the 1950's with concentric conic sections that reflect the x-rays at grazing incidence. Although the designs are relatively similar, the understanding of the residual effects of such a system have advanced very quickly throughout the last 30-40 years. For specialized applications, there has also been the introduction of a few novel methods that have allowed x-rays to be studied more closely. Multilayer mirrors which can now be manufactured within the necessary tolerances to make normal incidence reflection a viable option. Fresnel Zone Plates (FZPs) allow for diffracted x-rays to focus at a single point, but must be exceptionally small to properly diffract light with x-ray wavelengths. Compound Refracting Lenses (CRLs) consists of hundreds of small lenses, each of which bend an x-ray a very small amount, but together can focus a beam to a recognizable profile. All of these different focusing methods will be explored in this paper, from the theory of their operation, to their design, and to their manufacturing processes.

1 Background

1.1 Generation of X-rays

While the focus of this paper is on various methods of focusing x-rays, it is important to have a good background on how x-rays are created, both in space and in the lab. Figure 1-1 illustrates roughly where on the electromagnetic spectrum x-rays are located. Soft x-rays are called so because they have less energy than hard x-rays while gamma rays are beyond the scope of this paper. In general, x-rays are referenced by the amount of photon energy that they possess in keV rather than their wavelength.

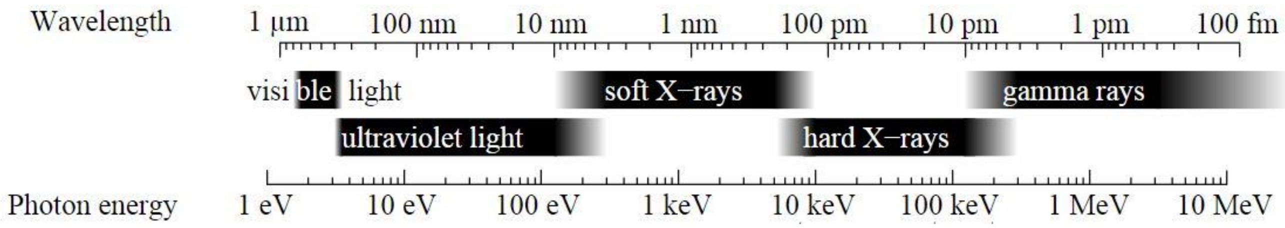

Figure 1-1: Spectral regions of electromagnetic radiation

Fundamentally, all blackbody sources follow the same law of emission, given by the equation

$$I(\nu,T) = \frac{2h\nu^3}{c^2}\frac{1}{e^{\frac{h\nu}{kT}}-1} \qquad (1.1)$$

The sun is the most easily recognizable blackbody source and has a temperature of ~6000°K. This gives a peak emission wavelength of ~555nm and the sun emits few x-rays by comparison. In order for a blackbody source to have a peak emission wavelength in the x-ray region of 10-.1nm, it would need to have an internal temperature of at least 10^6 °K. This is only attainable in large stars with very few heavy elements, very unlike the sun, similar to a supernova or black hole.

The next most common method of x-ray creation is with bremsstrahlung and characteristic radiation resulting from the impact of high-energy particles, or electrons. The bremsstrahlung radiation looks similar to black body radiation on a graph of power vs. wavelength and is relatively constant since it comes from the deceleration of the electrons as they interact with the atoms. The other, more interesting, type of radiation is the characteristic radiation that is a direct result of x-ray absorption by an atom and re-emitting a characteristic x-ray, illustrated below. These x-rays are unique to each element in the period table and can be easily seen in Figure 1-2. This is the method through which cathode ray tubes generate x-rays.

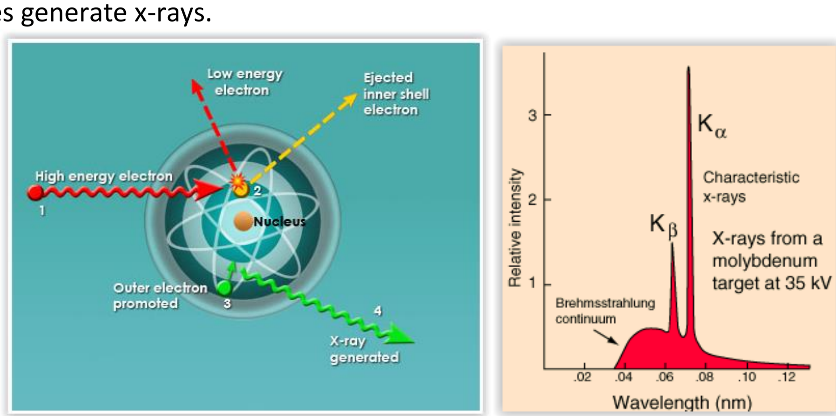

Figure 1-2: Generation and spectral characteristics of bremsstrahlung radiation

A final method, that is possibly the most inefficient, for generating x-rays is synchrotron radiation, although the x-rays that are created have extremely high levels of energy. This x-ray radiation is generated as a result of a charged particle, either an electron or proton, being influenced by a magnetic field. They were first observed in the 1950s as the first particle accelerators were created, generating for the first time fields that could create synchrotron radiation. They are emitted tangent to the curve in which they are travelling, as illustrated below. This allows for instrumentation to use the x-rays without interfering with the accelerator. Synchrotron radiation was initially waste from particle accelerators but began gaining popularity when it was realized that the waste energy could be used for experiments that require x-rays with a lot of energy. Since the discovery of synchrotron radiation, over 80 synchrotron sources have been developed, the most recent being commissioned at the Brookhaven National Lab in New York in 2015, with several more in development in Sweden, Brazil, and the Middle East.

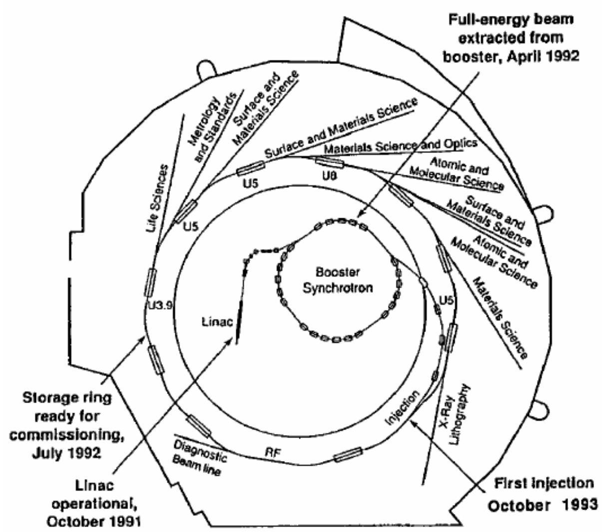

Figure 1-3: Synchrotron Source at Lawrence Berkeley Lab ALS

1.2 Discovery of X-rays

Wilhelm Röntgen discovered X-rays in 1895 [1]. As most great scientific discoveries, they were discovered by accident while Röntgen was working with cathode ray tubes. At the time, Röntgen was investigating the effects of cathode rays, beams of electrons generated in cathode ray tubes, on various materials. He discovered that even after creating a light tight system, one that would have blocked all cathode rays from exiting the tube, some of the objects in his lab began to fluoresce. This turned out to be because the fluorescing surfaces had been coated with barium platinocyanide, an early form of radium. The x-ray energy that was passing directly through his light blocking materials, were reaching the platinocyanide and energizing the electrons on its surface. With this information, he then created the first x-ray image, a shadow of his wife's hand in which her bones and wedding ring can be easily seen in Figure 1-4 [1].

Upon his discovery, Röntgen investigated whether or not these new x-rays could be controlled in the same way that visible light could via refraction, and he determined that lenses could not be used to focus x-rays. Until the mid-20th century, the properties of x-rays and their interaction with matter were not well understood, although pinhole imaging was used to create recognizable images, rather than simply creating a shadow of an object with x-rays.

Figure 1-4: The First x-ray image

1.3 X-ray Interaction with Matter

1.3.1 Index Decrement

The index decrement, δ, is by far the most important theoretical aspect of x-rays relative to this paper. A derivation is shown below to understand its physical origins, although the atomic theory is far outside the general scope of this paper. This is done because of the impact that the index decrement has on x-ray interaction with matter, for which a solid understanding must be built to design x-ray imaging systems. This analysis is drawn from a similar analysis that was performed by Spiller [2].

The index decrement comes about by the fact that EUV and x-ray energies are much higher than the band gap energies of almost all elements and compounds, while still imparting energy on the electrons that are bound by the atoms. The process that best describes this interaction is Thompson Scattering, where the input field is unchanged and the free electrons bound by the atoms are affected slightly. The analysis will be done by looking at the contributions to the field at a point in space, P, after a field interacts with a differential plane of free electrons with thickness d [2],as illustrated in Figure 1-5 [2], which closely resembles a smooth surface of the type that will be examined later in this paper.

Examining the energy that is radiated from the accelerated electron we see that the generated field is

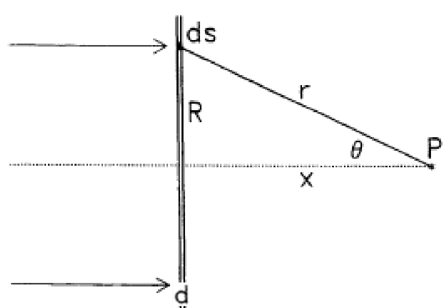

Figure 1-5: Generalized system for x-ray interaction

$$E_{electron} = -\frac{\Delta v}{\Delta t}\frac{e}{rc^2}\cos(\theta) \tag{1.2}$$

Knowing the acceleration of the electron due to the incident field, it can be shown that

$$E_{electron} = -\frac{E_0 e^2}{rm_e c^2}\cos(\theta) = -\frac{r_0}{r}E_0\cos(\theta) \tag{1.3}$$

Where r_0 is the fundamental radius of an electron in cgs units. This substitution will be important for verification of this derivation later. Since we are considering the differential area of an electron sheet with thickness d, and the fields that are generated from the accelerating electrons are spherical waves, the amplitude of the field at point P can be shown to be.

$$dE_{electron} = -E_0 r_0 \frac{e^{jkr}}{r} Nfd\cos(\theta)\,ds \tag{1.4}$$

Where N is the atomic density, f is the number of free electrons per atom, and k is the wavenumber. Expanding the differential area on the sheet in terms of r and defining $\cos(\theta) = \frac{x}{r}$ we can see that

$$E_{electron} = -2\pi E_0 r_0 Nfdx\int_x^\infty \frac{e^{jkr}}{r}dr \tag{1.5}$$

As the thickness of the sheet goes to 0, i.e. the sheet is only a single electron thick, $\int_x^\infty \frac{e^{jkr}}{r}dr = \frac{je^{jkx}}{kx}$ and the field contribution from the accelerated electron becomes

$$E_{electron} = -jE_0 r_0 \lambda Nfde^{jkx} \tag{1.6}$$

Since the incident field is unchanged in Thompson Scattering, its contribution to the total field at point P cannot be ignored, leading to the final field of

$$E_P = E_0 e^{jkx}(1 - jr_0\lambda Nfd) \tag{1.7}$$

Another method of examining the field at point P would be to examine the phase retardation of the field with respect to the index of the material.

$$E_P = E_0 e^{jk(x-\delta d)} \tag{1.8}$$

After differentiating with respect to d the following form is discovered

$$E_P = E_0 e^{jkx}(1 - jk\delta d) \tag{1.9}$$

Which closely matches the form of the field at point P when derived using the Thompson Scattering analysis. This allows us to conclude that

$$\delta = \frac{r_0}{2\pi}\lambda^2 Nf \tag{1.10}$$

The value of δ decreases quickly with decreasing wavelength, $\propto \lambda^2$, and is most prominent in the EUV and soft x-ray region. Into the hard x-ray region, the index decrement is on the order of 10^{-6} which makes it difficult to utilize. In general it can be seen that as the materials become denser, a higher number of atoms and a higher number of free electrons per atom, the index decrement will increase.

To verify this analysis of the index decrement, the complex index of refraction can be represented in the form

$$n = 1 - \delta - j\beta = 1 - \frac{r_0 \lambda^2}{2\pi} N(f_1 - jf_2) \tag{1.11}$$

Where f_1 and f_2 are the atomic scattering coefficients. Substituting the equation for the radius of an electron, in SI units rather than cgs units, the following form is seen for the index decrement.

$$\delta = \frac{Ne^2\lambda^2}{8\pi^2 \epsilon_0 m_e c^2} \tag{1.12}$$

Which is the exact same formula that is found in Michette [3] using the ideas of quantum absorption and scattering and that found in Lorentz [4] using the ideas of classical absorption.

1.3.2 Utilization of the Index Decrement

The x-ray index of refraction can be described in the following manner: $n_{xray} = n - \delta + iB$ where δ is the index decrement and β is the absorption index. The absorption index is only included when dealing with the transmission of refractive x-ray optics, so when looking at refraction or reflection, the real portion of the index is all that is necessary and it is simply $n_{xray} = n - \ \delta$. The index decrement is positive for all x-rays, albeit very slightly (10^{-6}) , leading to an real index of refraction that is less than unity. Having an index that is less than unity is what gives rise to the interesting system configuration that are described later in this paper. Reflecting optics are used at grazing incidence because Total External Reflection (TER) occurs at angles that are near 90° incidence from the surface normal. This follows the same theory that is used for Total Internal Reflection (TIR) with materials that have indices of refraction that are greater than unity. Following Snell's Law:

$$n_1 \sin(\theta_1) = n_2 \sin(\theta_2) \tag{1.13}$$

In cases with total reflection, the greater of the two indices is listed as being n_2.

$$\theta_{critical} = \sin^{-1}\left(\frac{n_1}{n_2}\right) = \sin^{-1}\left(\frac{1-\delta}{1}\right) \tag{1.14}$$

Gold, a commonly used material for reflective x-ray optics, has a $\delta = \ 1.88 * 10^{-5}$ [5] which gives a TER angle of $\theta_{critical} \geq 89.65°$. Refractive optics can also be used, although because the index of refraction is so close to unity, hundreds of lenses may need to be used in order to realistically focus the x-ray beam. This will make the absorption index a much more important property to consider. The many methods that are used to exploit the index decrement of x-rays are discussed in this paper in detail, analyzing their theoretical benefits and weaknesses, as well as their manufacturing feasibility.

1.4 Diffraction

The Huygens-Fresnel principle is based on the idea that any wavefront can be represented as an infinite sum of spherical wavefronts with a constant phase. Whenever a wave is being generated or altered, the wave can be represented on the surface that is altering the wavefront as an infinite sum of point sources as shown in Figure 1-6**Error! Reference source not found.** [6].

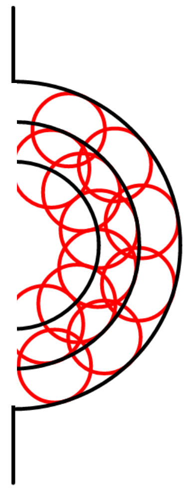

Figure 1-6: Illustration of the Huygens Fresnel Principle

Now consider slit such that when light is incident on it, it will diffract in a manner that is consistent with the Huygens-Fresnel principle. In the slit, each point source is infinitely small and infinitely close to its neighbors, and as they propagate, their phases will accumulate relative to the distance that each of the individual waves has travelled. There will obviously be some point at which the waves from neighboring point will interfere with each other, both constructively and destructively. In Figure 1-7 [7], the phase from each of the Huygens wavelets is independent of the one that is next to it and the path to the first angle where they have destructive interference is illustrated. This line has a phase shift of $m\lambda + \frac{\pi}{2}$. Each of the points along that line will have a phase of $0, \frac{\pi}{2}, or\ \pi$, which will mean that the peak of one wavelet will coincide with a trough of another. This concept is applied constantly in diffraction calculations as it is the defining characteristic of how the system will behave.

If this single slit were to be replaced with multiple slits that were infinitely thin and separated by a distance d, they would interfere in a similar manner. For this geometry, the waves will have a constructive interference when the observation angle, θ, is at a point where

$$m\lambda = dsin(\theta) \qquad (1.15)$$

Which is the commonly known grating equation. Destructive interference will similarly occur when

$$m\lambda + \frac{\pi}{2} = dsin(\theta) \qquad (1.16)$$

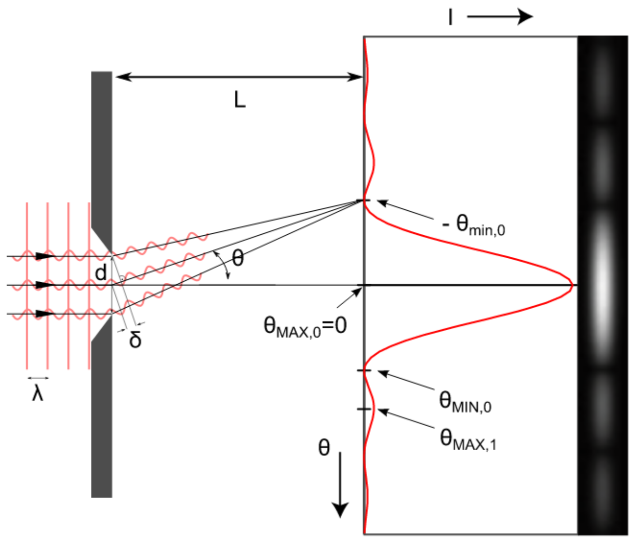

Figure 1-7: Illustration of Diffraction interference

1.5 Multilayer Coatings

Multilayer coatings are used when TER is either not realistic or not possible such as with very hard x-rays. These multilayer coatings are, in a much simplified description, a series of alternating thin high and low index material layers. Multilayer coatings take advantage of the Fresnel reflections that occur at each of these interfaces. Since the index decrement is so small for most materials, the Fresnel reflections are not particularly strong for each individual interface, requiring hundreds to over one thousand layers depending on the materials chosen. One of the methods that has been used with the multilayer coatings to improve their reflectance is to take advantage of Bragg reflection, shown in Figure 1-8 [8], which is a form of diffraction when the period of the multilayer is an integer multiple of the wavelength. Bragg reflection follows the same diffraction theory but instead of a plane wave being incident on a series of slits, the plane wave is incident on a series of layers.

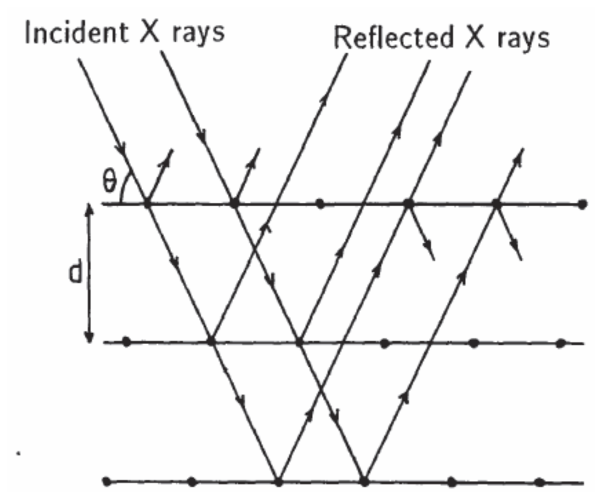

Figure 1-8: Principle of Bragg reflection

The same principle of interference occurring only at integer multiples of the wavelengths is true which is why the thickness of each multilayer follows the wavelength periodicity as explained by Equation 1.15. By creating a low-high index interface at that point, the Bragg reflection is intensified. The thickness of each of the layers within the thin film can be modified to achieve the desired performance, Figure 1-9 [8], as long as the overall period between each layer pair is the same and is an integer multiple of the wavelength.

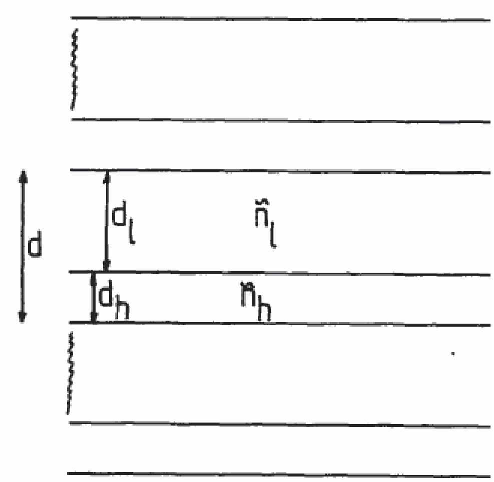

Figure 1-9: Varying thickness between high and low impedance layers for a thin film

There are several advantages to using multilayer coatings, primarily the reduced size of the system and increased aberration control, as a designer can use the same general design process as visible optics and the system can be folded. The main drawback from the use of multilayer coatings is that the transmission level is significantly lower. This is partly because the amount of light that is reflected at each surface is highly dependent on the difference of the indices of refraction, which are by definition very close to each other in the x-ray spectrum. The other part is because the materials that have very high δ values, making their reflections higher, also tend to have very high β values. Multilayer coatings have been introduced primarily in microlithography and microscopy applications, due to the reduced size of the system. These systems can use multi-layer coatings because the power of the source can be controlled to a much higher degree and is far more powerful than the objects being imaged in astronomical applications. Using multilayer coatings for most astronomical applications is not realistic since the sources being imaged are inherently dim as they are light years away.

1.6 X-Ray Spectroscopy

With the majority of the methods described above working over a broad spectrum of x-ray energies, it is important to be able to select the energy region of interest when it comes to the analysis. In most x-ray imaging systems this selection is done after the x-rays have been focused, but before they have been detected, with x-ray spectroscopy. There are many different techniques which use x-ray spectroscopy to determine the amount of energy coming from a specific wavelength, which can be very useful in determining the chemical composition of an object and could be the topic of a research paper in and of itself. This paper will only briefly describe the main methods of x-ray spectroscopy which are used in imaging systems. In the case of x-ray imaging, as is the case with visible systems, the driving requirements are both a high level of spectral and spatial accuracy. The two most common methods which have been employed in imaging systems have been x-ray detectors, either proportional scintillation counters or CCDs or, more prominently, x-ray diffraction.

The absorption methods have been used in imaging systems and often have good spatial resolution, but do not have very high spectral resolution, which is in many cases just as, if not more, important. This is because these devices work by differentiating between the voltages that are generated by each absorbed x-ray, similar to a visible detector, which can be difficult as this is limited to the resolution of the electronics and their relative noise, requiring the detectors to be cryogenically cooled.

The diffraction methods are much more widely used, as they take advantage of the law of diffraction described earlier. The focused broad spectrum is reflected off of a crystal lattice with a well-defined structure, and each wavelength is reflected at a different angle. This method is significantly more accurate, as the limit is the spatial resolution of the detector, which can be controlled to a much higher degree than the electrical noise. The image that is detected at each wavelength is then combined with the other wavelengths to create a final image.

A newer type of pixelated detector that is currently being developed for spectroscopy is the micro calorimeter array [9]. This method of spectroscopy uses minor temperature variations to determine the incident photon energy rather than variations in the electrical signal. While this design allows for a much more compact spectrometer that would not require as much alignment as a diffraction crystal, current implementations of this design need to use very sophisticated cooling systems that require the use of liquid Helium.

2 Grazing Incidence Systems

Utilizing TER is by far the most common method for focusing x-rays and will make up the majority of this paper. There are many different designs that can be implemented to take advantage of TER, evolving from their discovery in the late 1940s. Of those designs, Wolter optics are the most common and more analysis has been performed on their properties than any other type of grazing incidence design. One of the most useful aspects of the grazing incidence designs is that they are broadband reflectors. Since the index decrement becomes smaller as the x-ray energy increases, there will be an upper limit to the wavelengths that can be focused, which can be addressed with multilayer optics and is discussed in the next section. Each of the grazing incidence designs have their specific applications, which will be investigated and compared in this section.

2.1 Kirkpatrick-Baez Optics

Originally conceived in 1948 by P. Kirkpatrick and A. F. Baez, this was the very first imaging method for x-rays that focused light via either refraction or reflection [10]. At the time their paper was published, the general properties of x-rays and their interaction with matter were beginning to become well understood with regard to the index decrement and absorption index. The use of refractive lens systems was abandoned early on, primarily because of the fact that 100 consecutive lenses with radii of 1cm would still have a focal length on the order of 100 meters for a material with a δ on the order of 10^{-6}, which is considered large for most materials. This combined with the fact that most materials with a large δ also have a high β. Bragg reflection had been used for many years to determine the surface quality of a crystalline surface, but using diffraction severely limited the amount of light that could transmit through the system and would require a perfectly manufactured crystalline surface. These were the driving factors that lead to the design of a reflecting system that took advantage of the effect of TER.

The theoretical analysis of the Kirkpatrick-Baez design initially investigated only a single spherical surface. This single surface system was dominated by astigmatism and distortion, because of the grazing angle of incidence, while the other aberrations were relatively well controlled. This design was expanded to consider two cylindrical surfaces that would focus the light separately in each direction, controlling the astigmatism directly. The resulting Kirkpatrick-Baez design that is still in use today which consists of two spherical surfaces that are perpendicular to each other as shown in Figure 2-1 [10]. The

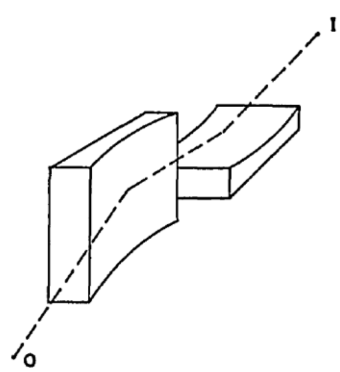

Figure 2-1: Original Kirkpatrick-Baez grazing incidence reflection design

imaging performance can be improved by using aspheric sections rather than strictly cylindrical sections, although this was not discussed in the original Kirkpatrick-Baez paper.

The expansion of the Kirkpatrick-Baez design to increase the collection area provides a direct connection to the Wolter type designs as well as the lobster eye designs, both of which will be discussed in detail later in this section. The main idea is that since there is only one plane in which there is any focusing of the light, a doubling of the collecting area can be achieved by simply adding another focusing plane next to that surface. In order to prevent each mirror pair from focusing to different locations, they are oriented such that they are both curved away from the same central line as shown in Figure 2-2 [11]. Because each of the mirrors must be focused to the same point, they will need to be aligned along slightly different axes as they move farther from the center line. This idea is directly related to the lobster eye designs.

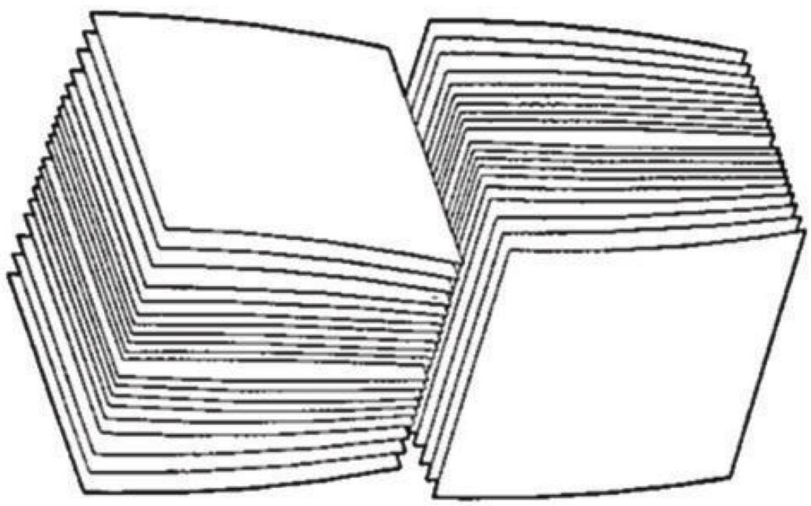

Figure 2-2: Stacked Kirkpatrick-Baez Design

The general Kirkpatrick-Baez design has many advantages, primarily that each of the mirrors can be positioned independently from both the other mirror and the focal plane in order to control the third order aberrations directly. The main drawback in this design is that the mirrors are spatially separated, which creates anamorphotism since each of the mirrors has a different object-image pair which leads to a different magnification in each direction. Because the two mirrors are spatially separated, they will also create 3 images, one from each mirror individually as well as one that is from the combination of their reflections as shown in Figure 2-3 [10]. At the time, the generated image was limited more by the grain in the film being used than any of the optical aberrations that had been considered, since each individual part of the system was tilted and shifted to make sure that the optimal image was created on the film plane. In an effort to further improve the design and use a film plane that is normal to the optical axis, a third mirror was introduced to create a symmetrical system as shown in Figure 2-4 [10]. Creating a symmetrical system removed any higher order distortion and coma, and also fixed the issue of the anamorphotism. By removing these residual aberrations, the field size was also increased dramatically.

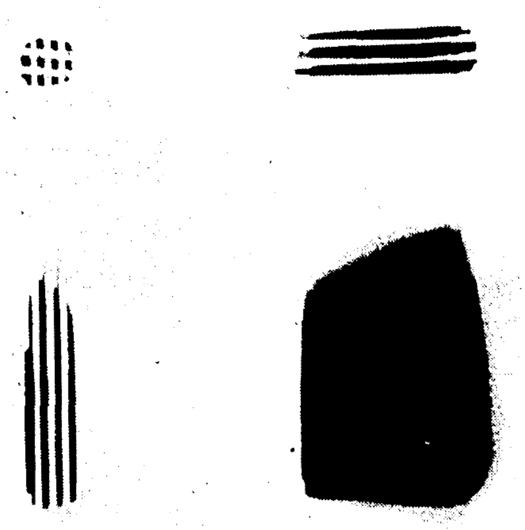

Figure 2-3: First images of a wire gauze pad with the first Kirkpatrick-Baez reflecting system

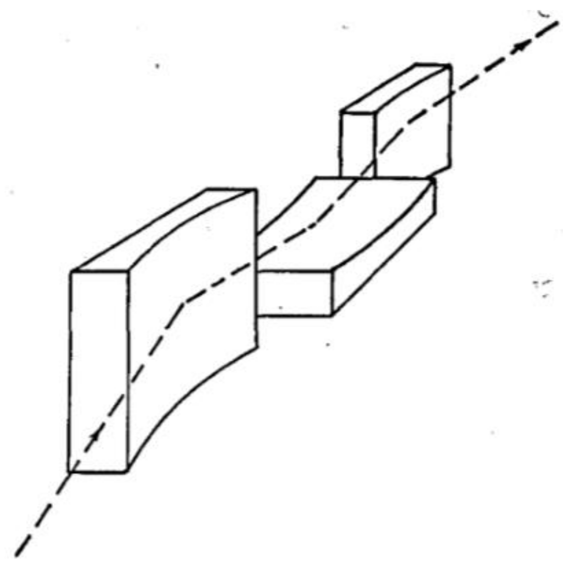

Figure 2-4: Improved Kirkpatrick-Baez Design with symmetry

The use of Kirkpatrick-Baez optics has been almost entirely limited to laboratory work because of the small collecting area and the fact that they are designed for point-to-point imaging. Some of the first sounding rocket imaging missions did have a Kirkpatrick-Baez telescope on them although this was primarily due to the fact that they were easier to manufacture at the time [11]. Kirkpatirck-Baez optics are still in use however because of their variability with alignment and their ease of manufacturing.

2.1.1 Montel Optics

In 1956 M. Montel devised a method which fixed the main issue in the Kirkpatrick-Baez design of alignment of the cylindrical surfaces, while simultaneously eliminating the anamorphotism [12]. This was accomplished by bringing both of the spherical mirrors together, so there was not any spatial separation and they had an intersection line where the two spheres contacted each other, Figure 2-5 [12]. Often these are referred to as nested Kirkpatrick-Baez optics because of their similarity.

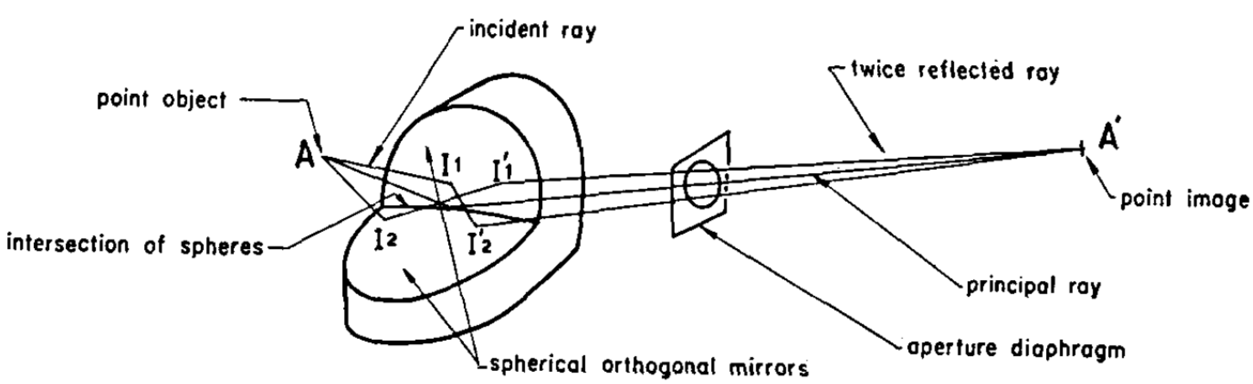

Figure 2-5: Montel grazing incidence reflection design

The imaging performance of this combination of mirrors was greatly improved [13], although the manufacturing difficulty was increased due to the fact that the line in which the spheres intersected is curved itself as shown in Figure 2-6 [12]. This caused the realistic increase in performance to be only approximately 2/3 of the theoretical increase predicted.

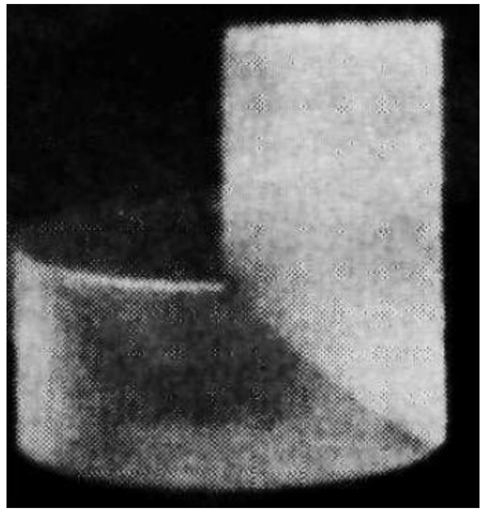

Figure 2-6: Image of Montel mirror configuration

There are very select instances in which a Montel configuration, mostly because of its compact design. Although the original design expected that the mirrors should be perfectly perpendicular, there have been experiments that demonstrate otherwise [14]. As recent as 10 years ago, the perfect perpendicularity was not questioned in depth because there has been little historical exploration of this design [15]. This deviation from expectation is mostly due to the fact that there is no defined reflection order from the two mirrors in the system. The rays can reflect off of the surfaces in any order, and the focused beams that they produce are not perfectly perpendicular to each other, some mirror tilt must be introduced to correct for these inherent errors. These minor tilts are shown in Figure 2-7 [14] and are derived from the reflection vectors for each surface.

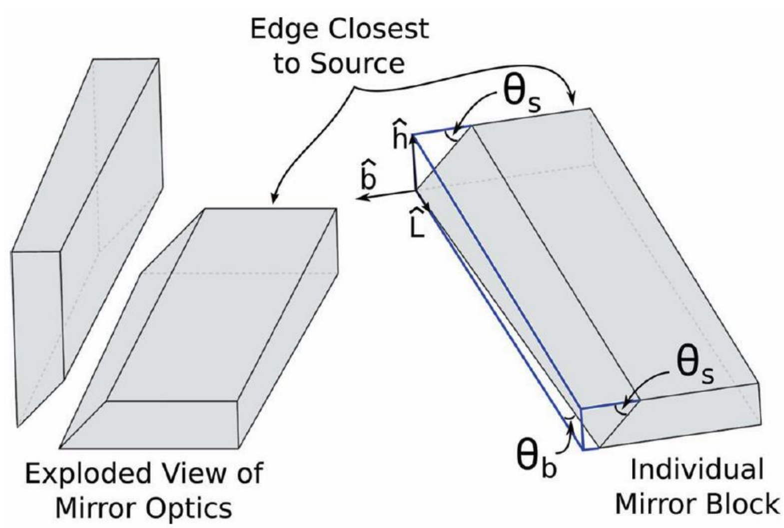

Figure 2-7: Improved Montel orientation

2.2 Wolter Optics

Wolter type optics were first created to solve the issue of axial asymmetry in the Kirkpatrick-Baez optics and they were conceived several years before Montel optics. Wolter type optics consist of a combination of rotationally symmetric conic sections that reflect at grazing incident angles. The use of multiple conic sections allows for a drastic increase in the imaging properties compared with the cylindrical optics that were originally used in the Kirkpatrick-Baez designs. All of the variations of the Wolter designs are selected because they fulfill the Abbe sine condition. While the sine condition can be fulfilled for a normal incidence reflection from conic sections, part of why they are used so heavily for visible and infrared imaging, grazing incidence reflections from an odd number of surfaces cannot [16]. Using an even number of surfaces is the only way to properly fulfill Abbe's sine condition with the use of grazing incidence reflections, and using any more than two mirrors presents a large engineering challenge with respect to the alignment and scattering losses [16].

While these designs have far superior performance to both the Kirkpatrick-Baez and Montel designs, they present the exact manufacturing and alignment difficulties that the other designs were designed to avoid. Although Montel optics were designed afterwards, they fixed the issue of any post manufacturing alignment, which has plagued Wolter optics from their inception. The level of asphericity is dramatic as the sections are not very close to their apex, which makes the proper manufacturing a great challenge. One of the largest challenges comes from the need to nest the different mirror combinations to increase collection efficiency. This is a necessity since the actual reflecting area of the mirrors is greatly reduced by their grazing incidence, as was the case for the Kirkpatrick-Baez designs. For example, a mirror that is 1m in diameter will appear to have a collecting ring with a diameter of only 6mm at the grazing angle of incidence calculated for gold in section 1. This reduces the collecting area by a factor of over 80x. The required nesting also creates the added challenge of creating a slightly different asphere for each nesting level.

One of the more important design considerations for Wolter Type designs is making sure that the conic sections that are selected will both have a coincident focal plane. This means that the first mirror images from one of its conic focal points onto one of the focal points of the other conic section that is used. Without this general layout of the conic designs there would not be perfect on-axis imaging.

Another effect of having such grazing incidence angles which reduce the overall collecting area is that diffraction becomes an important factor [17]. During early designs of Wolter telescopes, diffraction was ignored because of the very low wavelength that is being imaged as diffraction is directly proportional to the wavelength. Since the collecting area is a small annular ring, the telescope can be compared in some ways to that of a normal incidence telescope with a central obscuration, such as the Hubble Space Telescope, the only difference being the obscuration ratio. While the obscuration ratio of the Hubble Space Telescope is close to 0.18, the obscuration ratio for the Chandra X-Ray Observatory is just over 0.99. As is discussed by Harvey and Gressler [18], the diffraction pattern for a reflecting telescope with a given obscuration ratio ϵ can be calculated to be

$$I(x) = \frac{1}{(1-\epsilon^2)^2}\left[\frac{2J_1(x)}{x} - \epsilon^2 \frac{2J_1(\epsilon x)}{\epsilon x}\right]^2 \tag{2.1}$$

Where $J_1(x)$ is the zero-order Bessel function of the first kind.

Inserting this equation into math software leads to some interesting results, especially when looking at the effects of such high obscuration ratios as shown in Figure 2-9.

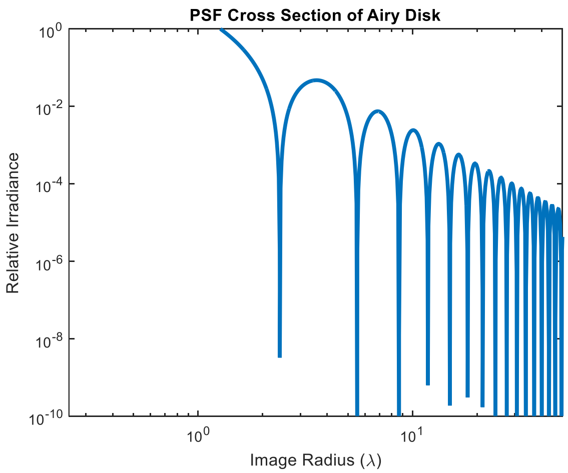

Figure 2-8: Calculated fringe pattern for telescope with an obscuration ratio of 0.2

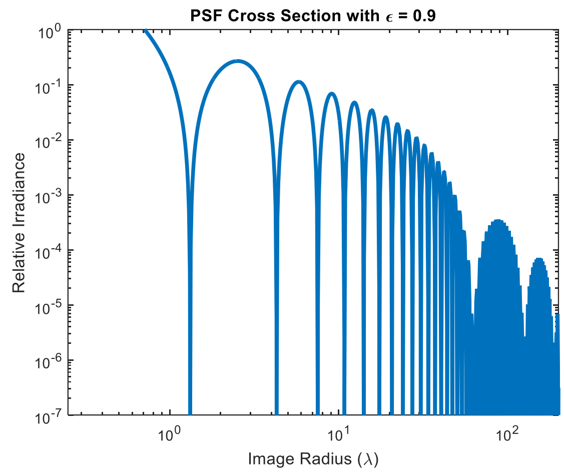

Figure 2-9: Calculated fringe pattern for a telescope with an obscuration ratio of 0.9

One of the known effects of having an obscuration ratio for normal incidence telescopes is that it reduces the size of the central airy disk. While that is true in the strict sense of the size between the optical axis and the first zero irradiance point, another pattern emerges in which a "secondary" airy disk begins to form. Within this secondary disk, which has a much larger central disk, there are the "original" airy disk rings. The first lobe is still smaller than the regular airy disk, 55% of the airy disk radius, which fits the theory that is known for smaller obscurations, and the rings outside of the initial lobe have significantly higher energy than before. This leads to the effect shown of having "ring groups". These groups appear similar to the airy disk, and in fact can be fit to a function that is a modified $sinc^2$ function as shown below. This meshes well with our typical theory, as the airy disk can be modelled as an unmodified $sinc^2$ function.

2.2.1 Type I

Wolter Type I designs consist of two conic sections in which the focal point of the first conic is behind that of the second, Figure 2-10 [19]. This leads to the incident rays having very shallow angles of incidence as the rays are gently being focused by each mirror. Such shallow angles of incidence require the systems that have abnormally long focal lengths, even compared to the other Wolter type designs. The conic sections will have a contact ring which can be used to aide in the alignment of the system, although it does not remove all of the alignment difficulties. Wolter Type I designs are by far the most commonly used for x-ray telescopes as they can be easily nested hundreds of times without any of the nested layers blocking the reflections from any of the outer layers, see Figure 2-11. All of the major x-ray telescope projects that have not imaged the sun have been with a modified Wolter Type 1 design, changing the specific aspheric parameters depending on the application. By having higher grazing incidence angles, Type I designs can also better image hard x-rays, especially with the combination of multilayer optics, a method that will be described in the next section.

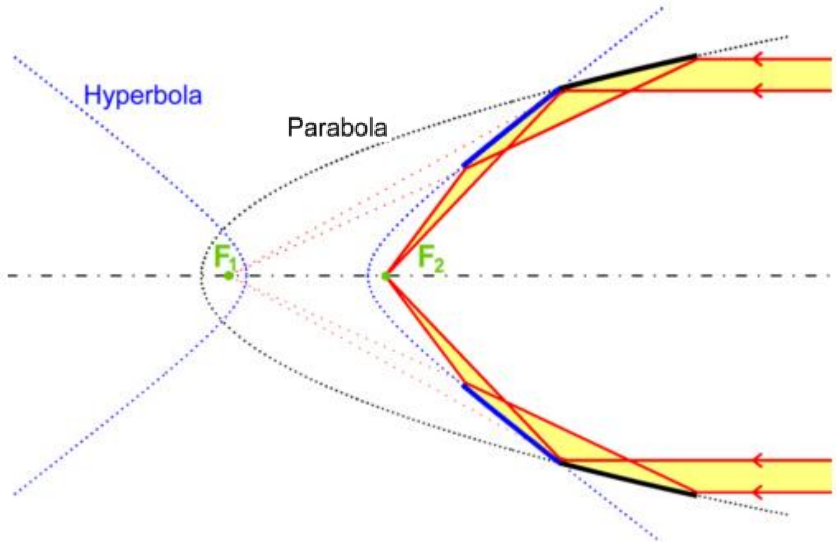

Figure 2-10: Wolter Type I mirror configuration

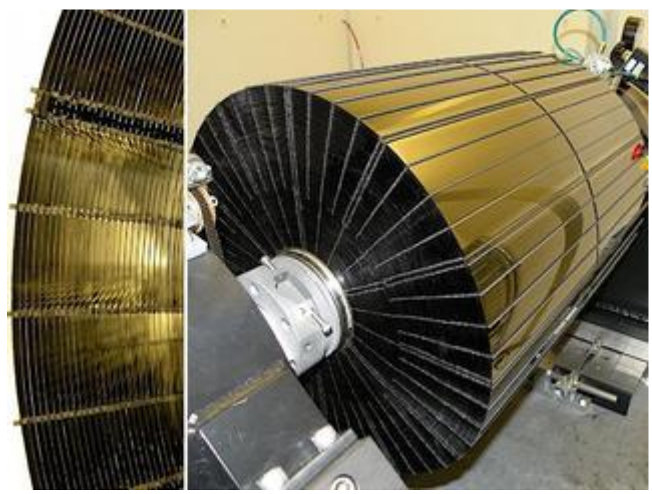

Figure 2-11: NuSTAR nested mirror assembly

Courtesy NASA/JPL-Caltech

Comparing Wolter Type I optics to a normal incidence visible telescope, the most direct comparison can be made to a Couder telescope, which uses a concave parabola and hyperbola to create an image [20]. This design is not as desirable as many other normal incidence designs because it creates its image between the primary and secondary mirrors, making it more difficult to access. Couder designs also do not have the added physical benefit of having a reflection from a positive and negative mirror, which is useful in cancelling many of the odd third-order aberrations.

While the designs of Wolter type telescopes are still evolving, similar to how normal incidence telescopes were evolving through mid-20th century, there have been significant improvements in their design over just the last 20 years.

2.2.2 Types II and III

Wolter Type II and III optics still consist of two conic sections, although in these designs, the focal point of the first mirror is actually inside that of the second, requiring an internal reflection and an external reflection. This modification leads to higher incident angles, which can only be used for softer x-rays. Because the focal points are reversed from the Type I designs, the aberration control is slightly better, similar to how using positive and negative lenses in combination work better to control even aberrations. Specifically, Type II designs have a positive first focal length that is shorter than the second. Type III designs have a negative first focal length and a positive second focal length. Examples are shown below. [19]

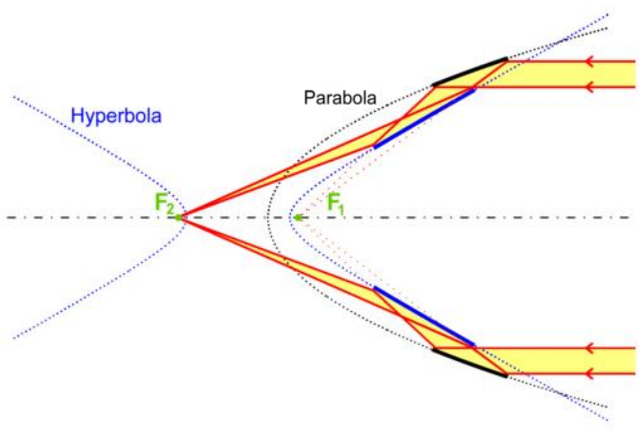

Figure 2-13: Wolter Type II mirror configuration

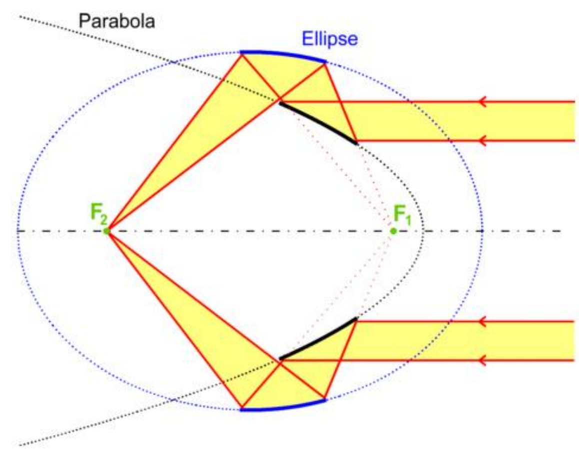

Figure 2-12: Wolter Type III mirror configuration

The Wolter Type II design has found some use in higher energy x-ray microscopes because its longer over all focal length allows for slightly higher magnification and the generalized use of an ellipse rather than a parabola also allows a point to be imaged from a finite distance rather than requiring a plane wave to be incident on the primary.

2.2.3 Design

There has been a significant amount of analysis of the overall imaging performance of the Wolter Type designs because of their usefulness in the field of astronomical x-ray imaging. Before examining the third order aberration theory for these telescopes, a thorough first order design and analysis must be completed. There have been multiple methods for which the first order design of a Wolter type telescope has been examined [20] [21], although many of them are only applicable to specific designs. Saha [22] has created a generalized first order set of equations that can be used on any grazing incidence reflecting telescope that is any combination of conic sections, and can be applied to any reflective grazing incidence system. Wolter originally described only 3 types of telescopes, while Saha expanded this to a potential 8 different telescope designs that could be designed using reflecting conic sections with the first surface being a paraboloid. Here, his analysis is applied to the Wolter Type-1 design.

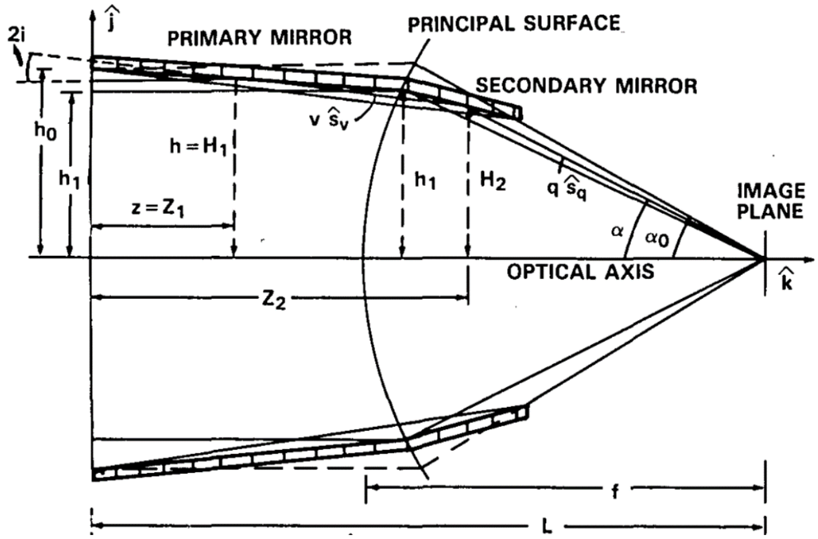

Figure 2-14: Parameters for a first order design of a Wolter Type-1 telescope

The general design parameters are shown in Figure 2-14 [22]. The equations that are created from these parameters examine a few properties of the rays that are being imaged through the system. These include the tangent of the reflected angle from the first mirror, i, a generalized sine condition for the surfaces of interest as derived by Saha [23], Fermat's principle of each ray having the same optical path length to the image plane, and the actual coordinates and directions of the rays once they have passed through the system.

$$\frac{dh}{dz} = -\tan(i) \tag{2.2}$$

$$s = z + v + q \tag{2.3}$$

$$h = \frac{2ftan\left(\frac{\alpha}{2}\right)}{1 + ntan^2\left(\frac{\alpha}{2}\right)} \tag{2.4}$$

$$L\hat{k} = h\hat{j} + z\hat{k} + v\hat{s}_v + q\hat{s}_q \tag{2.5}$$

Solving for the differential equation for h in both the $\hat{\imath}$ and $\hat{\jmath}$ directions leads to the following equations that can be uniquely defined for any grazing incidence telescope.

$$R_1 = \frac{2f(s-L) - h_0^2}{s + L - 2f} \tag{2.6}$$

$$R_2 = 2f\frac{s^2 - L^2 - h_0^2}{4f^2 - 4fs + h_0^2} \tag{2.7}$$

$$\varepsilon = \frac{4f^2 - 4fL - h_0^2}{4f^2 - 4fs + h_0^2} \tag{2.8}$$

Where R_1 and R_2 are the axial radii of curvature of the conic sections and ε is the eccentricity of the second mirror. The only values that are needed to determine the entire first order prescription are the desired aperture size, the focal length, system length, and OPL of any given ray, which can be easily calculated with the other known parameters.

2.2.4 Imaging Performance

This first order design prescription has been used since it was derived in that early 1980s because of its relative simplicity. Because this theory operates on the principle of having coincident foci of the conic section, it has a very small field of view since individual conic sections do not have very good imaging properties off-axis. This concept has also been an issue with normal incidence Cassegrain telescopes, which is why their original design has been modified over the years to increase their field of view but maintain improved imaging performance over spherical reflectors [24]. This is why almost all normal incidence astronomical telescopes are now of the Ritchey-Chrétien type, with both a hyperbolic primary and secondary mirror. The use of two hyperbolas for grazing incidence imaging, reduces the on axis performance slightly, Figure 2-15 [24], but greatly increases the operational field of view since spherical aberration correction is balanced between both mirrors. This idea was introduced to grazing incidence telescopes in the late 1990s by Harvey and Thompson [20] on the Solar X-ray Imager, and expanded on with the inclusion of Krywonos and Saha [25]. This new design was completed using an optimization routine in optical modelling software that maintained several properties of the telescope, such as the focal length and clear aperture, but altered the conic constants and central radii of curvature. While the off-axis imaging performance is not increased nearly as much as with normal incidence telescopes, the alignment errors are significantly reduced since the aberration correction is balanced between two surfaces. This benefit will be discussed further later in the paper.

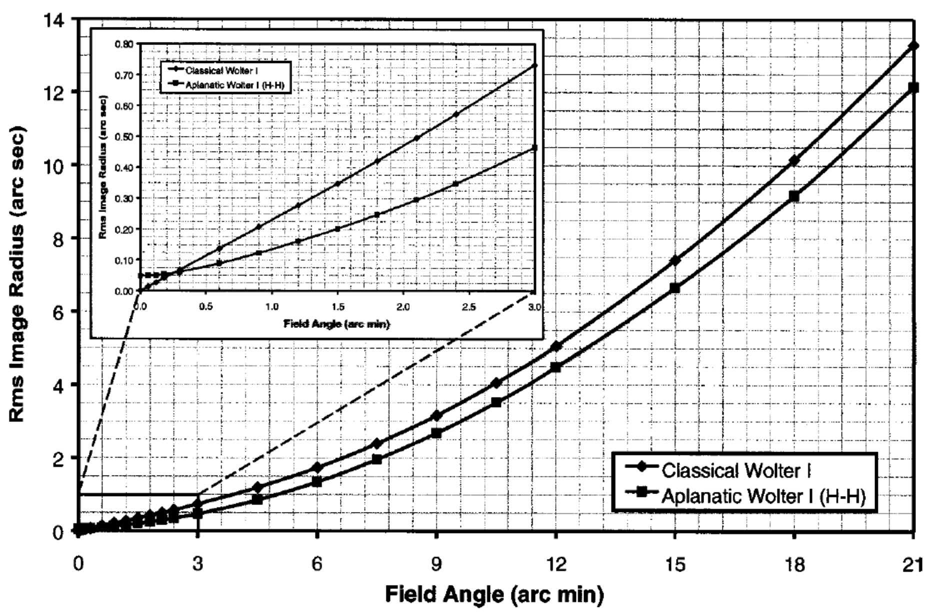

Figure 2-15: RMS spot size for the aplanatic and classical Wolter Type-1 Designs

With their prevalence in astronomical imaging, it is important to know the aberration performance of a grazing incidence system. Classical aberration theory does not explicitly consider grazing incidence systems, which makes their proper application difficult in this regime. There has been surprisingly little work that has been done to expand this theory so that it can be applied in the grazing incidence regime, although it has been done [26]. All of the third order aberrations have also been calculated, both with this method and without, so that they can be applied to the grazing incidence regime [27]. As with much of the theory that has been developed for x-ray telescopes, some of it is only applicable to Wolter style designs with a parabolic primary [28].

It has been shown that when spherical aberration is corrected for, coma is also driven to zero, and the dominating off-axis aberration is field-curvature over astigmatism and distortion, although they are not zero [27] [28]. This matches well with the fact that the original designs for Wolter type telescopes were aplanatic. The residual field curvature presents a difficulty in the design of these imaging systems as it is not able to be post-processed out of an image as it is field dependent defocus. The parameters that can be manipulated to reduce field curvature, such as increasing the diameter of the largest shell or increasing the focal length, also have their drawbacks with an increase in manufacturing difficulty and cost. As calculated by Winkler and Korsch [27], if there is a small amount of spherical aberration, then the field curvature can be reduced. This can be seen in Figure 2-15 where the field curvature is reduced by a seemingly constant amount, with the reduction of on-axis performance at the image plane, which can only be because of spherical aberration.

As is the case with normal incidence telescopes, third order theory does not fully explain the system performance, but it does offer some valuable insight in to the dominating effects. Exact ray tracing is still a useful tool in the evaluation of the system performance and will always give a more exact solution to the image accuracy. This is greatly aided by the use of the optical design software, which is now able to handle these complicated grazing incidence systems.

2.3 Flat Mirrors

Lobster-eye designs are a relatively new design when it comes to imaging systems because their structure was not understood in crustaceans until the mid-late 1970s. There are two main design types of lobster-eye optics which are analogous to the Kirkpatrick-Baez and Montel designs for spherical imaging at grazing incidence. There is the Schmidt design [29] which uses a horizontal and vertical array of flat mirrors, both of which are curved about the same point so that they create an image at the same location and the Angel design [30] which more closely resembles the imaging design of crustaceans, Figure 2-16 [11].

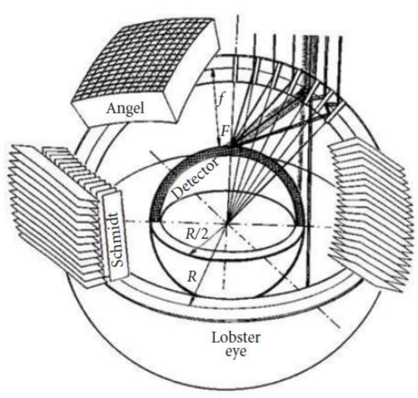

Figure 2-16: Various lobster eye mirror configurations

Both of these designs do not “focus” light in the same sense as any of the other grazing incidence designs because they simply operate under the law of reflection on a planar surface. By all of the planar mirrors being arranged perpendicular across a spherical surface, their angles of incidence will all be different, and their reflections directed towards the focal point.

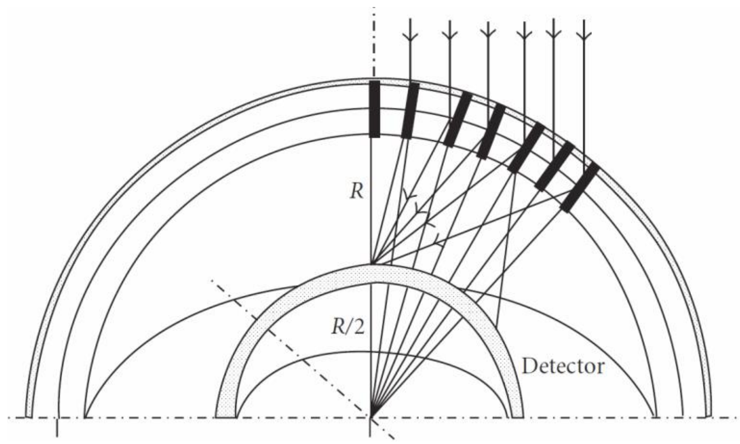

Figure 2-17: Schematic showing the focus of a lobster eye

It is important to note that the ideal detector surface is a sphere in all of the lobster eye imaging scenarios. This presents an interesting engineering challenge as curved CCDs have not been manufactured to date and film has become almost completely outdated. By only placing a detector at the focused location shown in Figure 2-17 [11], then only one direction is being imaged, which defeats the main benefit of the lobster eyes being able to focus light from all directions. To work around this issue, it is possible to scan the detector over the spherical surface and stich the images together [31]. An image from a flat CCD centered at a focal point is shown in Figure 2-18 [11].

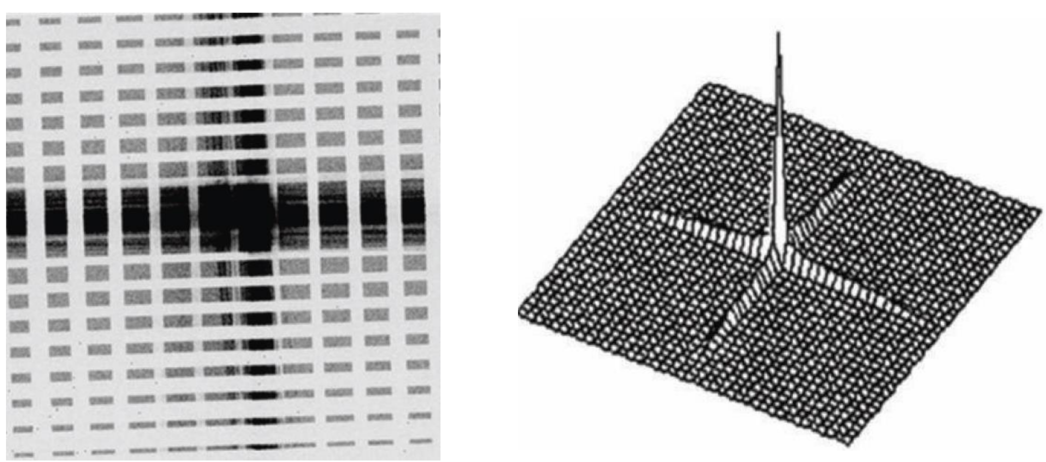

Figure 2-18: Focal plane image for a Schmidt objective (left) and its mathematical predictions (right)

The general form of the image is reminiscent of the Airy pattern, although the image is clearly not a diffraction limited spot of the rectangular aperture. The fact that there is no focusing involved, does reduce the resolution of the image, only allowing a resolution of a few arc-minutes with flat mirrors [32]. This can be improved upon however by taking the concept of the stacked Kirkpatrick-Baez design, and instead of orienting them on a rectilinear grid, orient them as if they were the flat mirrors in the Schmidt design [11].

In contrast with the Schmidt design, the Angel design would be much more difficult to manufacture with non-planar mirrors. In the Angel design, a cell array of planar mirrors is curved slightly and evenly over its area, so that it too would focus light to a curved surface. A magnified image of the cells are shown in Figure 2-19 [11], where the manufacturing issues are highlighted by the errors in where many of the larger cell blocks are combined. With the Angel design, there are few methods in which the cells can be manufactured, which is why they have not been studied to the same extent as the Schmidt objectives. The most recent technique that has been used is electroform plating and selectively growing each wall layer by layer, rather than milling out each section [33].

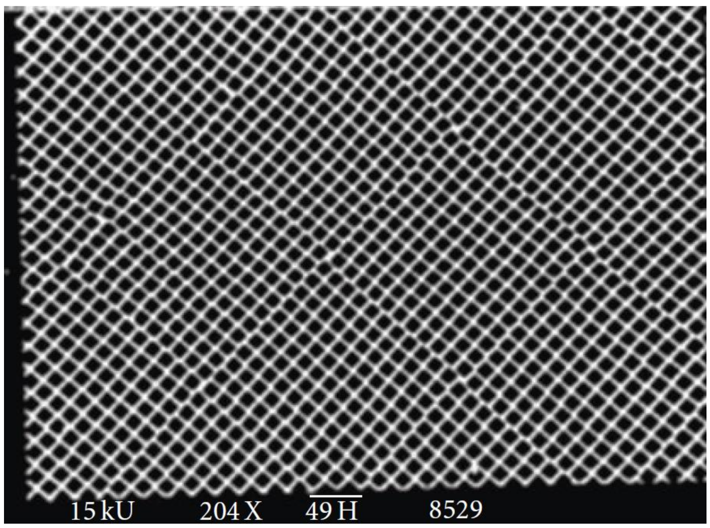

Figure 2-19: Cells in an Angel Objective

Because the Angel design does not require any extra housing components, it can have much smaller reflecting cells than can the Schmidt design and also reduces the overall weight, making it more appealing to space missions. This alone allows it to increase the resolution by almost an order of magnitude, to several arc-seconds rather than several arc-minutes [34].

Both of these designs are still in their relative infancy when compared to the Wolter and Kirkpatrick-Baez designs, although their potential is significant. They can theoretically image a 360° field of view, as long as it can be detected and with some slight modifications to their original designs, can have very similar imaging resolution to the older designs. The application of a multilayer film is not particularly useful here, because the angle of incidence from any one mirror varies depending on where on the spherical detector plane the actual detector is.

3 Normal Incidence Systems

All normal incidence optics for x-ray energies must use multilayer films. As has been discussed previously, this is because x-rays have minimal interaction with most materials due to their high energy levels. Since visible light has a significantly lower frequency, when it is incident on a metal, with a large number of free electrons, those electrons are able to resonate at the same frequency as the incident beam and re-emit (reflect) the incident wave in the opposite direction. Some of this light is absorbed however, which leads to different metals having different reflectivities. With the high frequencies of x-rays, the electrons cannot resonate as quickly and create more of a scattering effect which was derived in Section 1. This prevents regular reflection from occurring as would be expected from a metal so multi-layer coatings must be applied to make use of Fresnel Reflections at each surface. These reflections are based solely on the index difference and are highly inefficient with respect to reflected energy, although it allows classical optical design a possibility. Systems with normal incidence reflections have a tighter tolerances placed on them due to the lack of foreshortening that occurs from the grazing incidence but can create systems that have much greater optical performance. It is for this reason that the drawbacks are tolerated for highly sensitive systems such as those that are used for lithography applications.

3.1 Multilayer Theory

In the visible wavelength region, the most common method of achieving high reflectance with multilayers is by constructing a quarter-wave stack. A quarter-wave stack is illustrated in Figure 3-1 [35], where each material is alternating with high and low admittance.

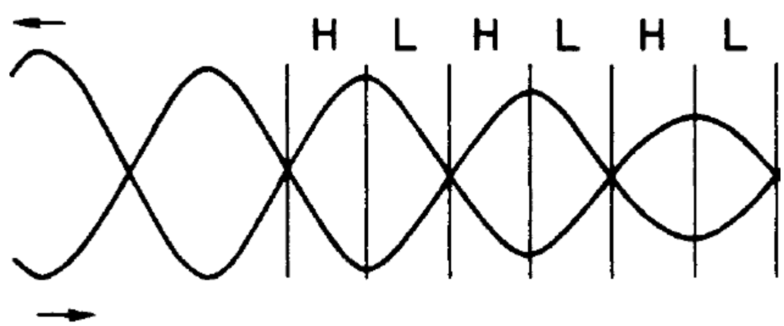

Figure 3-1: Standing wave pattern in a standard quarter wave stack

Admittance can be thought of as an index of refraction that accounts for the effects of the magnetic field as well as that of the electric field. Because of the fact that all visible optical frequencies are very high, the effect of the magnetic field on any medium can be neglected since it will not be able to interact with the electrons of the material. At very low frequencies, this cannot be ignored, but since x-rays have even higher optical frequencies than visible optics, to the point where the electric field hardly interacts with the materials, this approximation is more than valid. By ignoring the effects of the magnetic field, the admittance of a material becomes equal to its complex refractive index. For x-rays, this index is highly complex and the absorption is abnormally high.

This high absorption presents a problem with the design of a quarter wave stack, because the amplitude of the wave will decrease significantly as it propagates through the stack, reducing the coatings overall reflectance. An improvement in this design was first discovered by Eberhard Spiller in 1971 in which the thickness of the high admittance layer was reduced significantly [36]. By keeping the high impedance layer but reducing its thickness, the Fresnel reflection coefficients are still applicable at each interface, but the loss is reduced since less time is spent travelling through the high absorption material. The generalized shape of this new multilayer structure is illustrated in Figure 3-2 [35].

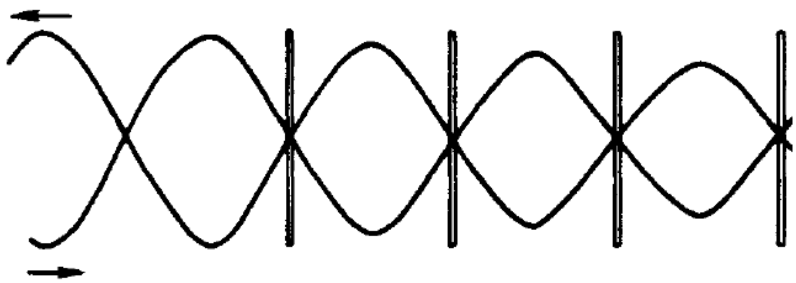

Figure 3-2: Standing wave pattern in a modified quarter wave stack

As with a regular quarter-wave stack in the visible, the more layers that are used in the multilayer, the higher the reflectance will be. In order to add more layers for high energy x-rays however, the thickness of the high impedance layer must be reduced even farther to allow for higher transmission [36]. At some point an equilibrium will be reached in which no more light can escape the multilayer due to it absorption and the reflectivity will not increase despite an increase in the number of layers that are in the multilayer. Figure 3-3 [36] illustrates this concept, which is the same for all energy levels. By maintaining the overall period of the multilayer structure, but minimizing the thickness of the high impedance layer to minimize absorption, a multilayer at normal incidence can reflect near 60% of the light at soft x-ray wavelengths, 130-140 Å, and near 30% for slightly harder x-rays, 60-65 Å.

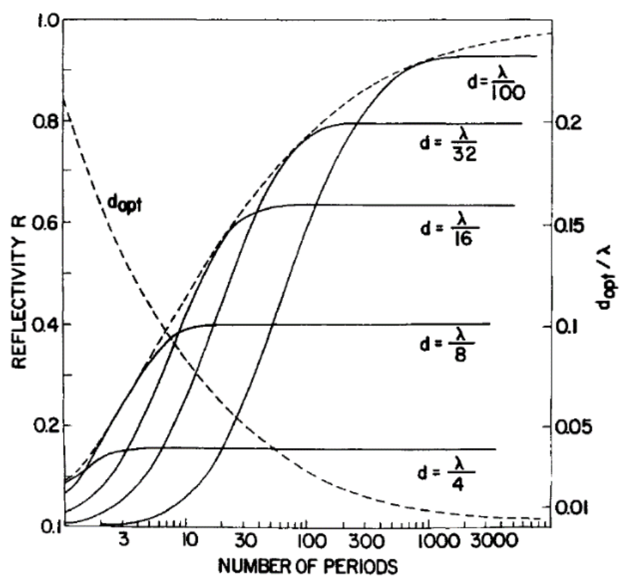

Figure 3-3: Calculated reflectance for varying thicknesses of high impedance layer in a modified quarter wave stack

Due to manufacturing constraints, it is very difficult to try to manufacture systems that operate at normal incidence below about 40 Å since the thickness of the absorbing layer would need to be on the order of 5Å, only a few gold atoms thick, to achieve reflections of just 20%. This is shown in Figure 3-4 [37] with a calculation of the ideal thickness of a Gold-Carbon thin film at 46Å.

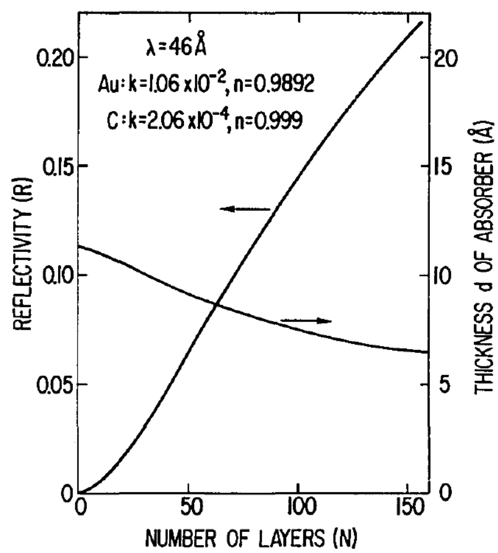

Figure 3-4: Calculated ideal thickness for a Gold-Carbon thin film stack at $\lambda = 46\text{Å}$

There are many design factors that need to be considered for normal incidence systems that are much different than those for the Wolter type designs. Since most normal incidence systems are going to be imaging a bright source, that is most likely at a finite distance away, and will not necessarily have a planar wavefront, the OPD from the top layer to the bottom layer as seen from the source is something to consider. If the OPD creates an angular separation that is less than the width of the reflecting peaks of the thin film, then the effect on the thin films reflectivity can be ignored [38]. Figure 3-5 [38] illustrates the angular considerations of this analysis. When the calculated $\Delta\theta$ is less than the wdith of the reflecting peaks FWHM, than the distance y is large enough to ignore the reflectivity differences at each layer.

$$\Delta\theta > \frac{Nd}{y}\sin(\theta)\cos(\theta) \tag{3.1}$$

Where N is the total number of layers. Using the numbers from [39], assuming a rocking curve angle of $0.25°$ and a worst case incidence angle of $\theta = 45°$, then we find that $y > 0.024mm$ which is an unreasonably close object for most imaging purposes. As was the conclusion in [38], this consideration is not of any practical concern for thin film imaging.

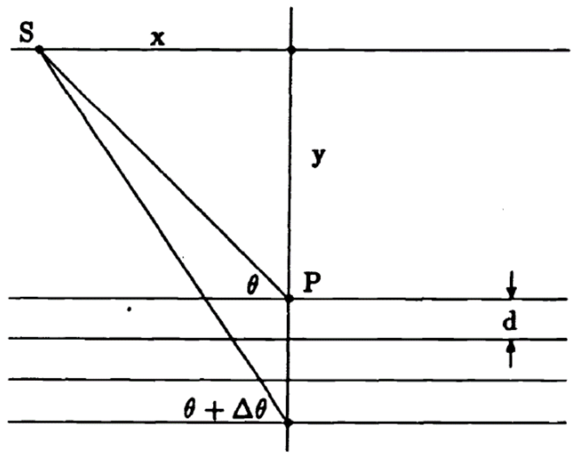

Figure 3-5: Angular OPD over the thickness of a thin film

Another consideration for thin film imaging conditions that is closely related to the angular OPD that was just described is how the curvature of a thin film multilayer would affect its focusing abilities. Since the angle of incidence at the surface of reflection with the index of refraction, the location of the formed image will also vary slightly. Figure 3-6 [38] shows the basic geometry for this analysis where I is the image formed from the reflection off of the first surface and I" is the real image formed from the reflection off of the second surface. I' is the apparent image location from the reflection off of the second surface without refraction.

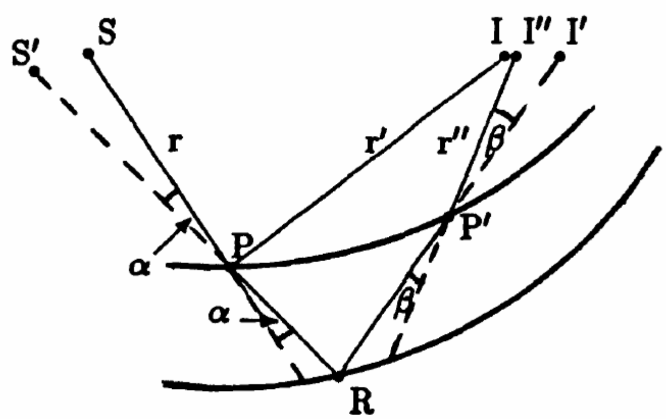

Figure 3-6: Curved multilayer imaging deviations due to index of refraction

To the first order, the approximation can be made that $r' \approx r$" since the thickness of each of the layers is less than one wavelength, and by the same approximation, that $\alpha \approx \beta$. With these simple first order approximations, it is clear that the distance between I and I' and that between I" and I' is the same, which means that minor variations in the curvature and thickness over the clear aperture of the optic will not have a significant effect on the imaging performance of the system.

As a final design consideration, and something that will be mentioned in much more detail later but has a significant impact on the imaging performance of the system is the surface roughness of the boundaries between each layer of the thin film. As the roughness increases at one layer, even if a perfectly smooth layer is deposited on top of it, the errors in the first layer will be present in the second layer. As the roughness of the reflecting surfaces are compounded, the reflective angles are no longer centered around the rocking curves of the multilayer because the integer multiples of the incident wavelength are now randomized over the entire coating. This drastically reduces the contrast of the image since rays that are coming in at any angle may be reflected towards the image plane but it also greatly reduces the image quality as the rays coming in at the desired angle are reflected generally towards the image plane but not in the designed manner. This topic will be discussed in depth in the manufacturing section of the paper.

3.2 Multilayer Imaging

In order to image hard x-ray energies, a combination of grazing incidence and multilayers must be used. The grazing incidence is utilized not because the reflectivity of the materials inherently increases due to the angle, as is the case with softer x-ray energies that can achieve TER, but due to the foreshortening of the multilayers at such high angles of incidence. The same theory applies that decreases the overall collecting area of the grazing incidence telescopes.

For a multilayer system to image hard x-rays that are 8 keV, 1.55Å, using the generalized quarter wave stack, the period of each of the multilayer pairs would need to be an integer multiple of .775Å, essentially impossible at normal incidence. While layers that are several integer multiples of .775Å would still have the same reflecting effects, the increased thickness increases the absorption significantly as well. This is made much more difficult by the fact that, as shown in Figure 3-3 [36], the high impedance layer will need to have a period that is significantly smaller than a quarter of a wave. At an angle of about 1° the thickness of this multilayer stack can now be extended to be over 40Å thick, which can be easily manufactured. As shown in Figure 3-7 [39], a reflectivity of near unity can be achieved at these grazing incidences with multilayer films, d is in Å. It is clear that the high reflectivity is only near the angles of incidence where the foreshortened thickness of the total period is an integer multiple of $\frac{\lambda}{2}$ and that the reflectivity is decreasing significantly for each of those integer multiples due to the increased depth that the wave must travel for each reflection.

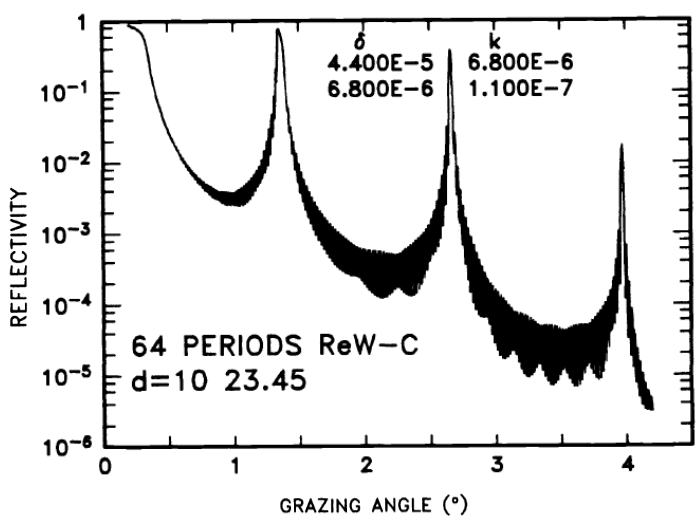

Figure 3-7: Calculated reflection as a function of incidence angle for a Rhenium/Tungsten-Carbon thin film with $\lambda = 1.54Å$

The use of multilayers at grazing incidence is on several space telescope already, its main benefit being that it can work at harder x-rays than can a single element coating or a bare substrate can. The drawback from this type of design though is that it only works at one specific and unchangeable wavelength of light. This makes the proper design of the system that much more important before launch on a space satellite as the wavelength of interest that is being imaged must be one that can provide valuable information.

To circumvent the issue of only being able to image a single wavelength, several telescopes with various coatings can be manufactured to image the same source. While this may appear to be quite costly, a clever method has been used on the Spectral Slicing X-Ray Telescope, SSXT, [40] where a Wolter Type-1 telescope was utilized as a broadband focusing optic, and a normal incidence interchangeable tertiary mirror was utilized as a spectrometer to focus the image onto the image plane. Figure 3-8 [40] shows how these interchangeable mirrors were placed on a rotating disk and each mirror was coated with a different set of materials to image 5 different spectral lines from the sun, ranging from 33-238Å.

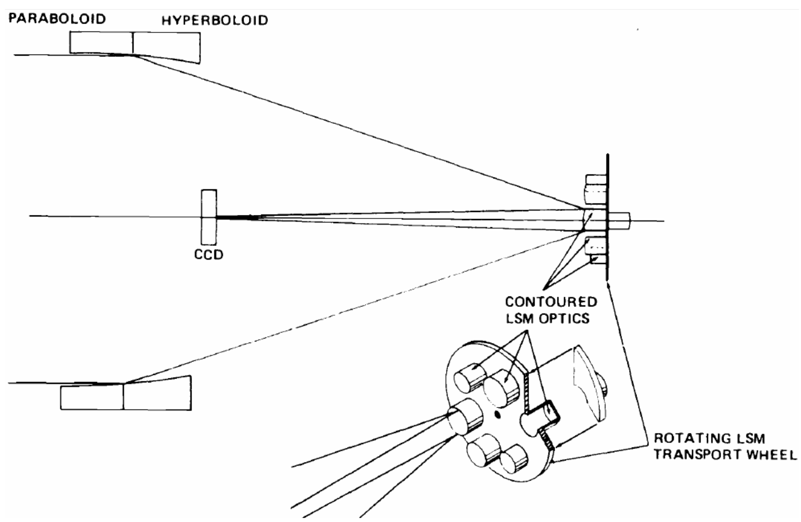

Figure 3-8: Schematic outlining the overall design of the SSXT

This design tackled several problems at once while improving the optical performance with the addition of a third mirror, selecting several desired spectral lines, which was often done with a more costly spectrometer near the detector, and also shortening the overall length of the design which is important for space flight. This is one of the few times in which normal incidence multilayer films have been used in space telescopes, as there are few reasons that they would have a benefit over the general broadband imaging of a Wolter type design. The use of a classical Wolter Type-1 design was also not a problem here, as it was for the AXAF project that was mentioned earlier, because the use of a spherical tertiary mirror greatly increased the functional field of view of the telescope.

Even with the increase in design restrictions with multilayer thin films, there are many benefits, some of which have already been mentioned. Primarily, there is the ability to maintain the system size of a normal incidence system. The fact that the hundreds of layers that can be present, do not have an adverse effect on the performance of the system means that classical third order analysis can be performed rather than requiring years of work to provide a new understanding to the old theory. The abnormal diffraction effects that were mentioned in the previous section on grazing incidence systems are also not a factor here, since regular two mirror systems can be used. Without this diffraction behavior, the limiting factor in the performance of the system becomes the geometrical aberration performance, rather than the diffraction characteristics. Since diffraction effects scale with the wavelength, using shorter and shorter wavelengths allows the designer to essentially ignore diffraction altogether when working with a normal incidence thin film system. This creates the interesting situation where many of the higher order aberrations must also be considered, as they will not be dominated by the effects of diffraction [41]. Using incident light with a wavelength of 20nm, very large in the realm of x-ray optics, diffraction limited performance is still on the order of 50-100nm even for a relatively slow optical system. It has been shown that resolution on the order of $0.1\mu m$ can be achieved using only spherical surfaces for finite imaging [42]. Figure 3-9 [42] shows the resolution potential using a Schwarzschild objective, a commonly used design for x-ray microscopes.

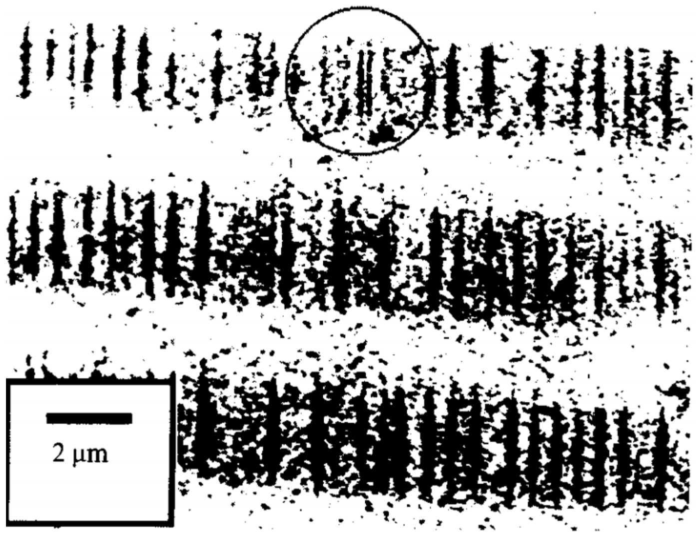

Figure 3-9: Image from a normal incidence microscope for $\lambda = 20nm$

4 Refracting Systems

The use of refraction to focus x-rays is only recently becoming feasible due to the manufacturing constraints that are required, although they are still not entirely practical for most applications. The materials that are used for refraction must be carefully selected to balance out their positive and negative properties. Refractive systems can only be considered in applications with high energy sources, and need to be carefully manufactured to maintain the theoretical performance.

4.1 Compound Refracting Lenses (CRLs)

CRLs are rarely used because of their manufacturing difficulty and accuracy. Due to the fact that the x-ray index of refraction of materials is so close to unity, there need to be many lenses that are all of very high curvature, $r < 1mm$. Because the index of refraction of the material is less than that of air, all of the lenses will need to be concave in shape, which goes against classical optics design intuition. When designing CRLs, an important ratio to consider is ${}^{\delta}/_{\beta}$, which will be called the refraction ratio. The higher the refraction ratio is, the more effective a lens will be at focusing an x-ray without absorbing too much of the energy. In general, the less dense the material, the higher its refracting ratio, not necessarily because of an increase in δ but rather a decrease in β since there is less material for the x-ray to be absorbed.

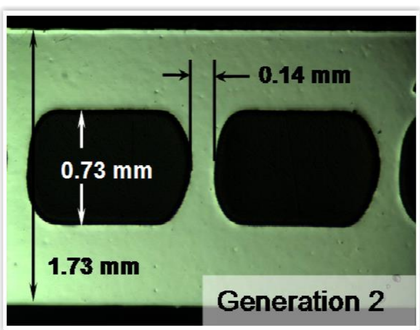

Figure 4-1: Magnified image of a CRL made of aluminum

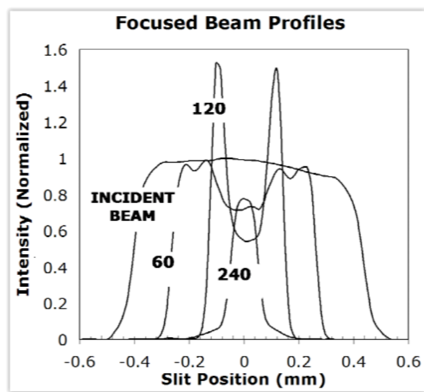

Figure 4-2: Beam profile of focused light with varying number of lenses in an aluminum CRL

CRLs made with aluminum [43], a readily available and easily manipulated material, would need 200+ lenses and would only lead to a focused spot that is about 1/3 the size of the input beam, and would have an intensity of about 75% of the input due to the high level of absorption with so many lenses. It is also important to note that the measured beam profile was more than 20m from the CRL array. This clearly has far less focusing power and far lower transmission than any of the reflecting telescopes that have been analyzed.

As can be seen in Figure 4-2 [43] a significant number of lenses are needed in order to properly focus the incident top-hat profile into a spot. When a similar experiment was performed with Lithium CRLs, a material that has a significantly higher δ and lower β [5], only 32 lenses were needed to achieve the same profile, while transmitting significantly more energy.

The use of CRLs is primarily limited to use in laboratories where overall size and cost is an issue, and where very high power x-rays can be generated, such as with a synchrotron. The faintness of the signals being measured in space eliminates CRLs as a possibility. Another issue with the use of CRLs is that each surface will need to be exceptionally smooth in order to not have compounded image errors from each surface interaction. It is difficult to see from the profile shown if there are any aberrations other than defocus that are present, although the shape of the focused beam appears to show that the imaging performance would at least be adequate. There have not been many investigations into the imaging performance of CRLs, only their ability to simply focus X-rays, due to the fact that there are many other, more easily accessible methods for actual imaging. If the manufacturing can be done in a cost-effective manner however, this could be a viable option for use in a synchrotron where the x-ray profile simply needs to be controlled rather than imaged as is the case for astronomical uses.

4.2 Prisms

Using a prism as a focusing method is an alternative to using CRLs and has many of the same practical issues including the significant number of prisms needed and the significant amount of absorption. Using prisms however, greatly reduces the manufacturing difficulty. Prisms can either be created to be rotationally symmetric, or they can be created as two sheets of prisms, which would lead to a line focus rather than a point. An rotationally symmetric example is shown in Figure 4-3 [19].

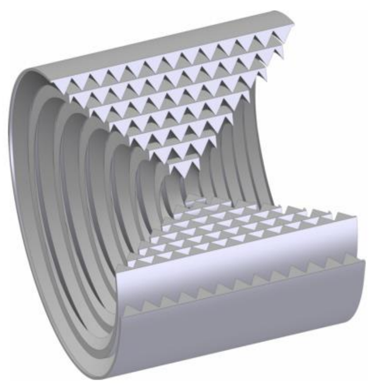

Figure 4-3: Rotationally symmetric prism focusing design

The usefulness of using refracting methods is debatable, but until they can have the same level of transmission, collection area, and optical performance as the reflective methods described above, they will not be widely implemented.

5 Diffracting Systems

As has been explained in previous chapters, while the effects of diffraction are reduced as the wavelength is reduced in regular imaging systems, they cannot be ignored when using abnormally high obscuration ratios. Investigating the use of diffraction as a method of dispersion/imaging rather than an artifact of a separate system is an entirely different proposal that will be explored in the following sections. Using diffraction at x-ray energies is not much more difficult that using them in the visible region, as the theory is exactly the same. As will be discovered in this section, and has been shown for other x-ray systems, the limiting factor comes in the choice of materials and their surface finish.

5.1 Gratings

Diffraction gratings are the most fundamental diffraction technique and are the most commonly used method for diffraction in the visible region. At its most basic level, a grating is a series of repeating structures, similar to the series of slits that were analyzed in section 1, that will either reflect or transmit light with a change in either the phase or amplitude of the incident wave. This can be used in a variety of different applications, but only those that can be used for focusing rays are discussed in this section.

In practice, using a series of slits is not desirable as the majority of the light that is incident on the grating is lost. More commonly, especially for x-ray applications, reflective gratings are used to diffract the light, as all of the light is reflected off of the grating. Reflective gratings come in many forms, perhaps the most straightforward extrapolation from the slit theory that was derived is a laminar grating shown in Figure 5-2 [44]. One of the more common reflective designs is that of a blazed grating, shown in Figure 5-1 [44], which uses a periodic sawtooth pattern rather than a periodic square wave pattern. As previously discussed however, in order to get a decent reflection efficiency from a material with x-ray energies, grazing incidence reflection much be used.

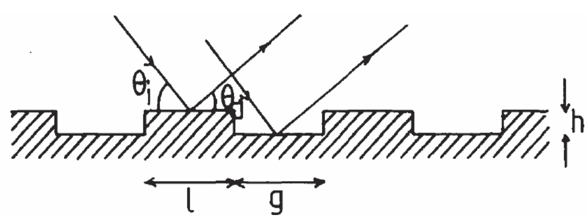

Figure 5-2: Binary grating pattern

Figure 5-1: Blazed grating pattern

As can be imagined, with grazing angles of incidence, the reflective gratings shown in Figure 5-2 [44] will cast a shadow on themselves, reducing the amount of light that will be diffracted, which in turn reduces their efficiency, but will also reduce the effective land area that the x-rays will see.

With visible light, the defining characteristic of the grating is the ratio of $\frac{\lambda}{d}$. As this ratio is increased, so is the amount of dispersion that is introduced, making it easier to select a specific wavelength after reflection. In the visible region, d is approximately 1-10 times the wavelength of interest, up to several thousand $\frac{lp}{mm}$. This ratio seems nearly impossible to manufacture for x-rays since they have such short wavelengths, but when accounting for the shortened landing size due to the grazing angle of incidence, the theory can be adapted so that the gratings can still be manufactured [44].

5.2 Fresnel Zone Plates

Fresnel Zone Plates (FZPs) can be thought of as simply a rotationally symmetric grating, with variable slit spacing and size. The variable spacing is used so that as the light is diffracted at the plate, it will be able to interfere and create an image at the same linear distance from the plate on the optical axis. The diffraction that occurs at the zone plate is described by the Bragg diffraction equation that was previously derived: $m\lambda = 2\ d\ sin(\theta)$ where θ is the diffracting angle. The fact that FZPs utilize diffraction, the plate can be thought of as a lens that has a different focal length for each wavelength. Because of this, chromatic effects are difficult to avoid with FZPs.

FZPs come in two very distinct types, those that modulate the amplitude, and those that modulate the phase of the incident wave. Amplitude modification is a slightly misleading term as these FZPs are still looking to selectively image certain phases that will interfere constructively at the image plane. This is achieved by simply blocking out the areas of the plate that will not contribute the proper phase, which leads to the labelling of an amplitude modification FZP. FZPs that modulate the amplitude are strictly binary in their form, half of the zones are transparent, while the other half are opaque (Figure 5-3) [45]. In order to select the areas of the plate that will contribute the correct phase to the image, the spacing of the rings must vary radially. This means that each opaque and transparent zones alternate when $s_n - f = \frac{n\lambda}{2}$, where n is the zone number and $s_n = \sqrt{r_n^2 + f^2}$. This leads to the equation of the radial thickness, r_n, of the nth zone to be:

$$\sqrt{r_n^2 + f^2} - f = \frac{n\lambda}{2} \qquad (5.1)$$

Which simplifies to

$$r_n = \sqrt{n\lambda f + \frac{n^2\lambda^2}{4}} \approx \sqrt{n\lambda f} \qquad (5.2)$$

For the very short wavelengths that we have with x-rays.

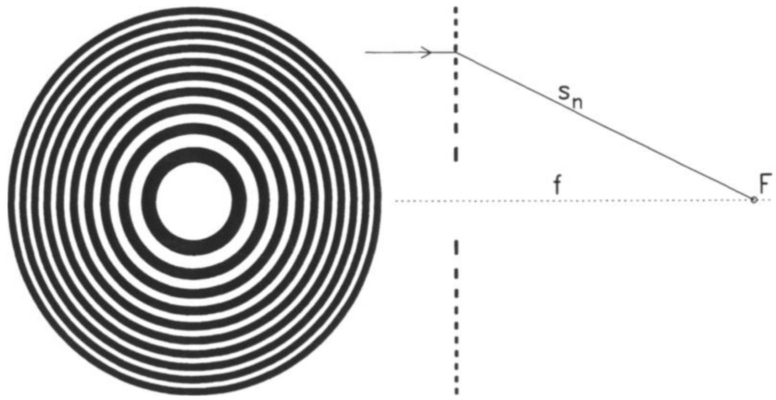

Figure 5-3: Generalized Fresnel Zone Plate (FZP)

Amplitude modification FZPs are a little easier to understand theoretically, however they are much less efficient since they block more than half of the light that is incident on the zone plate. Another problem in using amplitude FZPs is that the materials need to be carefully selected as the opaque zones need to be completely opaque. A fine balance also needs to found between thickness and transmission in order for an amplitude FZP to be realized. For this reason, phase modification FZPs have become much more prevalent in their use.

In a phase modification FZP, the zones are not strictly binary in their construction [46]. Each zone consists of 'steps' which vary their thickness depending on their location in the zone (Figure 5-4) [46]. This in turn varies the phase change that occurs after the incident wave travels through each step.

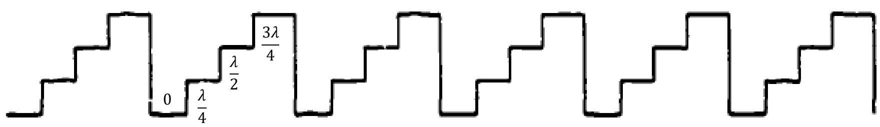

Figure 5-4: Discretized sawtooth wave for phase modification

These types of FZPs are attempting to replicate the general sawtooth pattern that would have a continuous phase shift over the width of each zone. As can be imagined, the more discreet phase levels that are present in each zone of the FZP, the better the realized performance of that FZP will be. The amplitude FZPs can easily be modified to become a phase FZP by simply changing the opaque material to a carefully selected material with a specific thickness that will create a $\frac{\lambda}{2}$ phase shift. The spacing of each zone will be determined by the formula

$$r_{n,l} = \sqrt{\lambda f \left(2\frac{l}{L} + n - 2\right)} \tag{5.3}$$

Where L is the total number of levels, 2 for a binary FZP, l is the level of interest within the total number of levels, and n is the zone of interest. In this case, n can only be an even number so instead of the zones being labelled 1,2,3, ... as before, the zones will be labelled 2,4,6, ... with everything else remaining the same. With a binary FZP, the formula simplifies down to $r_n = \sqrt{n\lambda f}$ as was derived previously.

The transmission efficiency would increase dramatically with a phase shifting FZP and the resolution would remain the same. The manufacturing process would need to change however, which could reduce the number of zones that could be realized.

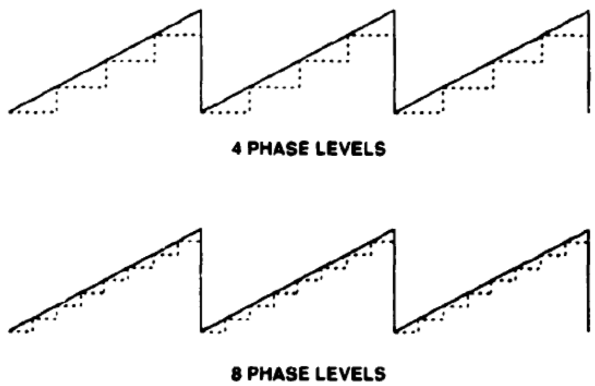

Figure 5-5: Increasing number of discreet zones in a sawtooth wave

The limiting factor in the accuracy of the phase FZPs is, just like the amplitude FZPs, going to be how thin each of the steps can be made. In general, the resolution of the phase FZPs will not be as high as that of the amplitude FZPs while their overall efficiency is increased dramatically. All of the same theory can be applied to the phase FZPs as they are still a periodically repeating structure whose period is radially varying. The only real difference between the two types of FZPs is how they are achieving the desired phase shift at any given point away from the center of the FZP. Obviously, the manufacturing processes involved in making the phase FZPs is more difficult, although the increase in transmission is often worth the increase in manufacturing since many x-ray sources are not powerful enough to throw away the majority of the incident beam and still have enough energy to detect an image with a reasonable exposure.

Since FZPs operate by using diffraction to alter the incident field for imaging purposes, by definition they have diffraction limited performance, meaning that the image that they produce is one of the airy disk with the first ring having a diameter of

$$r_{Airy} = 1.22\lambda \, {}^{F}\!/_{\#} \approx \frac{\lambda}{2NA} \qquad (5.4)$$

The resolution can only be improved by increasing the NA of the zone plate, which requires an increase in the number of zones, which means the spacing between the outer zones will become much smaller. This is generally the limiting factor in the design process of an FZP. There have been some significant and creative advances in the manufacture of FZPs, which have made them a much more feasible design with the ability to create significantly smaller zone widths for both amplitude and phase changing systems. These techniques are discussed in the following section.

It has been shown that a higher level of resolution can be achieved if the central zone of the Zone plate is blocked [47]. This would prevent any of the on-axis light from reaching the detector and spread out some of that energy into the lobes of the Airy disk, shrinking the central peaks FWHM. The main trade off here though is that the amount of energy that remains in the central lobe is only about 25% of the original amount. The counteract this effect, a composite zone plate can be used. These composite zone plate is a combination of two separate zone plates, one of which is designed as has been described to image the first diffracted order, and the other one having been designed to focus its third diffracted order to the same location. This is shown in Figure 5-6 [47], where it can be seen that by “starting over” with the zone spacing and thickness with a larger central radius, the third diffraction order is imaged as well. This also has the effect of increasing the resolving power of the zone plate by increasing the NA of the system. Composite zone plates can also be manufactured to image the fifth diffracted order as well, which would further increase the imaging performance.

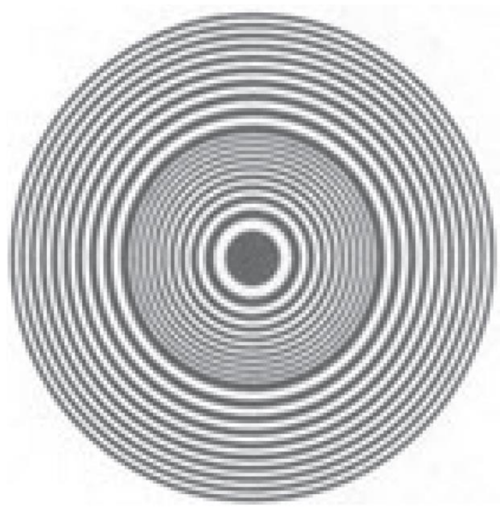

Figure 5-6: Composite zone plate with 40 zones

6 Manufacturing and Assembly

The first several sections of this paper have been dedicated to the optical imaging theories that drive the designs of each type of imaging optic. In reality however, there are always manufacturing constraints that restrict how accurately this theory can be realized. It was these manufacturing constraints that prevented Newton from building a parabolic primary mirror for the first reflecting telescope. While the theory had been around for many years that proved that the imaging performance of a parabolic reflector is far better than that of a spherical reflector, the technology did not exist that allowed the parabolic shape factor to become realized. In the same sense here, the majority of the constraints in the design and manufacturing of x-ray imaging systems, does not come down to the theory of the design, but rather the manufacturing and the assembly.

6.1 Reflecting Systems

6.1.1 Grazing Incidence

There are several different methods by which grazing incidence telescopes can be manufactured including the typical grind and polish techniques that are used for most visible optics applications, replication of a master blank, or by forming thin foils to the proper shape [48]. Each of these methods have their benefits, although one constant throughout all of the systems is that the roughness of the reflecting surfaces has a large effect on the final image performance [49]. Figure 6-1 shows a great summary of all of the surface metrics that need to be considered when manufacturing a grazing incidence system [50].

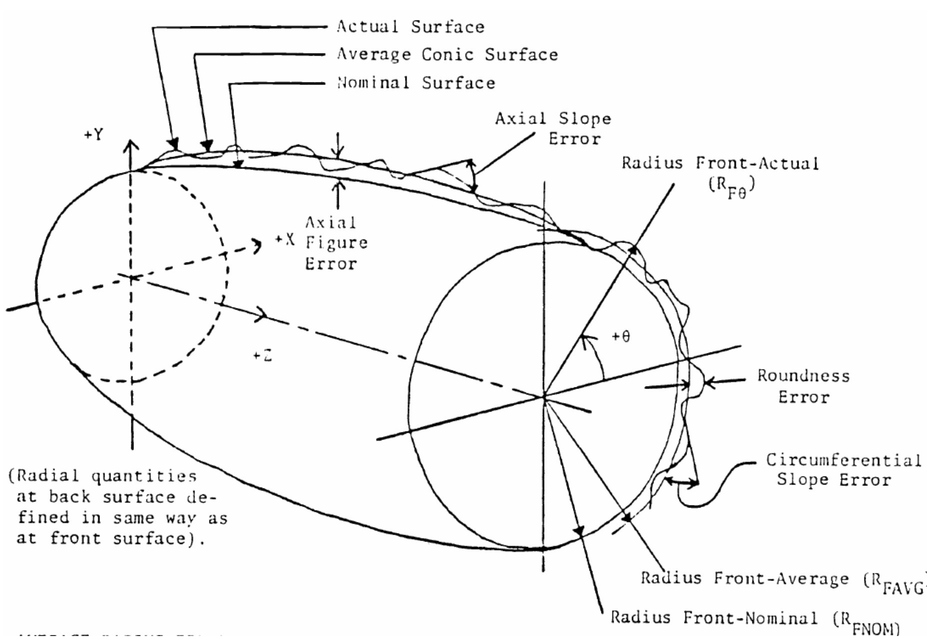

Figure 6-1: Surface metrics for a grazing incidence reflecting system

In the typical grind and polish technique, the glass blank that has been formed to the approximate shape of the final surface is shipped from the glass manufacturer. This is generally made to the approximate spherical approximation that is necessary for the conic sections. The final surface is polished down to make sure that the surface roughness fits to the proper specifications, often with a surface finish of less than 5Å [48]. The optics are quite expensive to manufacture due to the uniqueness of their general shape relative to most visible or IR optical assemblies. The equipment that is needed must be custom built for a one time use which is part of why x-ray telescopes are few and far between [48].

The grinding and polishing techniques can vary depending on which materials are being used for the original blank [50]. The blank does not need to actually be glass, since the final polished surface is often coated with a few layers of a single material thin film afterwards. As will be discussed later in this section, the finish of the substrate for a thin film is one of the most important manufacturing considerations. The choices that go into choosing the material for the optical substrate are its uniformity, weight, cost, and difficulty to change after original manufacture.

When it comes to large blanks, glass is actually quite difficult to manufacture with good uniformity since it is created in a high temperature environment and then must be cooled afterwards. Maintaining a uniform cooling over a large and thick piece of glass can be quite difficult which would cause internal stresses and strains that could reduce its overall performance [48]. Metal can be reheated and reformed much more easily than glass can so its uniformity is often better, although its ability to get precision surface metrics after the initial shape factor is created is notably more difficult. The typical process for polishing glass blanks can also get the surface roughness to a much lower level than that of metal polishing. Within the group of metals and glasses, there are always materials that are going to cost more, trying to make a general statement about which costs are worth the increase in performance is difficult and is a decision that should be made for each project. It is worth noting however that the cost of the testing methods should be included in that analysis.

To test these grazing incidence surfaces, the most commonly used surface metrology method for visible optics, interferometry, is not applicable in the same way that it is used for normal incidence optics. The methods need to be modified to more closely resemble the way that multilayer mirrors are measured at normal incidence. This is another part of the manufacturing and testing process in which the apparatuses need to be custom made. As shown in Figure 6-2 [50] the testing set-ups generally need to be inserted into the rotationally symmetric reflecting surfaces.

The major benefit to using the grind and polish manufacturing technique is that almost every aspect of the optics can be controlled to a very high degree. Because the process is very precise, some of the best astronomical images with respect to strictly the optical performance are taken with this type of x-ray telescope. This is far from the only viable technique however, as other methods have been used on high precision x-ray telescopes. Some of these methods, as will be described, are more desirable due to their cost and ability to alter shape after manufacture.

When using a master blank to create several replicas of the same mirrors, similar to the manufacturing procedure for most diffraction gratings, there is only a need to manufacture one version of the mirror with the ability to create multiple copies with the same performance [48]. The general manufacturing procedure for this master copy is very similar to the grind and polish technique that was just described. The difference comes from the fact that the masters are typically made out of some sort of metal which would allow a different metal that will be used as the reflector to be deposited on the master and then removed for use in the telescope.

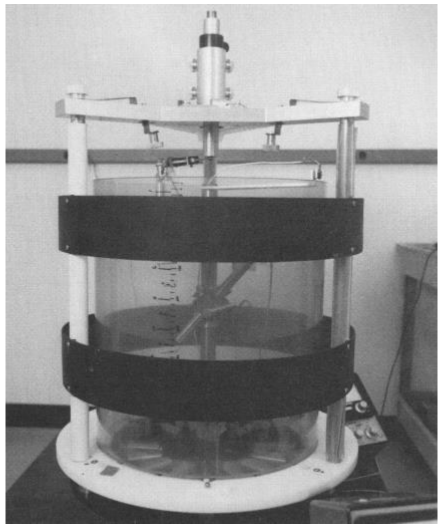

Figure 6-2: Surface profilometer used in the metrology of the AXAF project

This technique allows there to be a few copies of the same optics in a single telescope, as was the case for the Newton XMM and NUSTAR [51]. The increased number of mirrors allows for a larger effective collecting area which can then allow for fainter astronomical objects to be imaged. With these faint imaging systems, a common issue is the level of shot noise, which is directly related to the number of photons that are incident on the detector at any time [48]. By imaging the same object with multiple copies of the optics, the noise can be more easily removed and the image enhanced in post processing.

Another benefit of using the master blank technique is that each of the shells that is used as a reflector is much thinner and lighter than the glass counterparts that were used in the previous technique. Since weight is one of the driving factors for most designs that are launched into space, there can be a significant benefit from removing some of the weight with a different manufacturing technique.

The biggest drawback from these thin replicated foils is that there surface shape can be much more easily altered than with a large glass blank. If the alignment of each of the shells is not perfect upon installation, then it becomes much more difficult to align each one of hundreds of mirrors. The specifics concerning the alignment of the nested sections is discussed further at the end of this section.

The same internal stresses that are present from non-uniformities in the glass manufacturing process, can be found in these replicated sections as well. When the replicated shells need to be removed from the master blank, significant amount of stresses are put on the mirror, as it must be pulled off of the master blank. This is the point where significant amount of material engineering need to be considered so that removing the near perfect blank does not alter its overall shape and finish [48].

6.1.2 Normal Incidence

All normal incidence systems are made of multilayer thin films. The techniques for the creation of these thin films have improved dramatically over the last few decades, making this technique much more viable than it was when x-ray telescopes were initially introduced.

The first thin film deposition process that was used for creating thin films was Chemical Vapor Deposition (CVD). In this process, chemical reactions occur among several input gasses in which the desired material is separated from their inputs and essentially fall onto their substrate. This technique creates some of the most pure elemental depositions of any thin film deposition technique when the reactions are tightly controlled. It is for this reason that CVD has been so commonly used. The main issue with CVD is not its purity but it uniformity of deposition across the substrate. While the actual reaction rate of the chemicals is well known, meaning that the deposition rate is well controlled, the actual type of deposition is not directly controlled. Since the reaction is driven by the temperature in the chamber, higher temperatures will create a more uniform deposition. This is the issue that is highlighted in Figure 6-3 [52], where the temperature is decreased as the distance from the heating element is increased, which will reduce the uniformity. A method to combat this would be to increase the amount of gas that is being input to the system, although this supersaturation moves the deposition away from the desired epitaxial configuration.

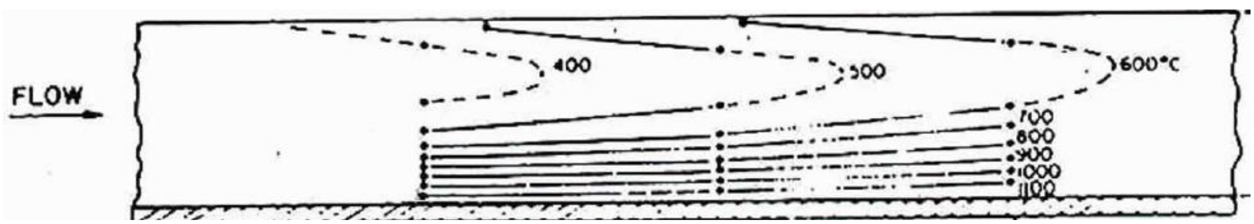

Figure 6-3: Chemical Vapor Deposition non-uniformities in the deposition across the substrate

A second method that has come into greater use in recent years is Molecular Beam Epitaxy (MBE). In the MBE process, a Knudson cell is filled with highly pure elements that will be deposited on the substrate. From these heated Knudson cells, a beam of electrons is directed onto the pure materials and they are evaporated onto the heated substrate. Because the beam of electrons can be well controlled, the rate of evaporation is also very well controlled. This allows for some of the most uniform and thin deposits of any deposition technique, as shown in Figure 6-4 [52]. This comes with a very high

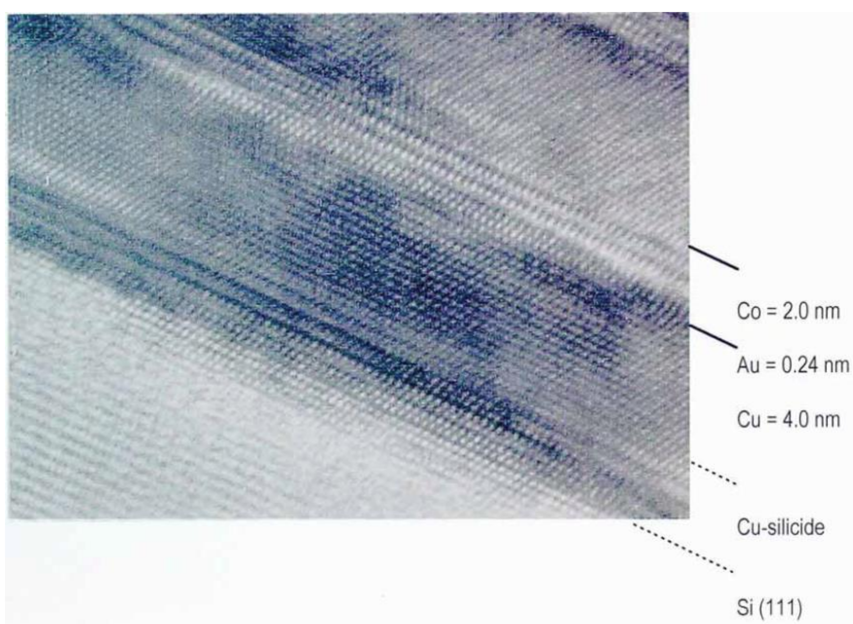

Figure 6-4: Cross-section of a thin film created with Molecular Beam Epitaxy

cost however, making a single basic machine on the order of $1-2 million without many add-ons for in situ measurements. Since the materials that are being deposited are evaporated from the Knudsen cell, their purity is dependent on the chemical process that created them. While this purity can be on the same level as those created in the CVD process, an ultra-high vacuum (10^{-8} Torr) [53] needs to be created in order for the purity of the substrate to be maintained. In the end, similar levels of purity can be achieved with CVD and with MBE and the significant increase in cost can be attributed to the increase in precision of the deposition.

In any type of thin film deposition, the main concern when it comes to the application of x-ray imaging is the smoothness of the boundaries between layers. This is related to both the surface roughness of each surface, which can be directly related to the surface roughness of the substrate, and the lattice matching of the materials that are used to make the film.

There has been much analysis related to the selection of materials to create the thin films [54] [53]. In Rosenbluth's tables, the only parameters that were considered were the complex refractive indices relative to their atomic scattering coefficients, as described in the first section. Falco expanded on this analysis by considering the lattice matching and elemental compatibility, specifically with MBE deposition in mind as that provides the most reliable film thickness and uniformity. The list of elemental candidates is reduced significantly when the actual manufacturing constraints are considered, down to approximately 5-10 different pairs of elements. Of these, the highest level of reflectivity, accounting for the absorption over the several hundred layers needed, is $\sim 50\%$ above 5nm and only $\sim 20\%$ once the wavelength is reduced to 3.5nm.

6.1.3 Alignment

The alignment procedures for the normal incidence and grazing incidence systems vary drastically. Since the normal incidence mirrors are so much more closely related to classical optics, their alignment procedures are very similar. In general, the difficulty of the normal incidence mirrors comes from their precise multilayer structures, whose precision has been already been discussed. The only alignment difficulties lie in the centration of the optics along a normal optical axis. As many of the materials that are used in the multilayer structure have high reflectivities in the visible region as well, the same or very similar equipment can be used to align each mirror along its necessary axis. Even off-axis conic sections can be aligned without much more difficulty than their visible counterparts. Because of this fact, the alignment difficulties and precision will not be discussed further.

The major difficulty in alignment comes with the grazing incidence systems. While their design has been discussed thoroughly, the entire aspect of mounting and aligning the nested sections has not been considered. Typically, the alignment considers two separate errors, the alignment of the primary and the secondary, which is a consideration of all two mirror telescopes, and perhaps more importantly the alignment of each shell to its nested neighbors. In the replicated foil telescopes, there is often no method for post assembly alignment due to the number of individual sections that there are to put together [55]. Once the larger groupings of the primary and secondary shells have been assembled, there will be an alignment procedure for combining them to make sure that they are within tolerance. Only in the larger assemblies such as the Chandra, where there are only 4 nested sections, will there be an attempt to adjust each mirror individually.

As has been mentioned previously, the system is designed to be aplanatic, and by the nature of their design, each mirror has negligible amounts of astigmatism and distortion. This means that the major alignment aberrations that will be seen are defocus and third order coma.

Typically, defocus will appear as a uniform image blur that has a growing radius as the separation from the ideal image location increases. In the case of the concentric shells, the radius grows in the same fashion, but the image is no longer a uniformly illuminated circle but rather just a ring with the same radius since there is such a high obscuration ratio. There will be one ring that will be made from each of the individual shells from the telescope.

As for third order coma, the image will also consist of a grouping of rings of different radii. The typical geometrical aberration looks similar to a comet with a large tail but with this telescope configuration it will not be a continuous pattern as shown in Figure 6-5 [55].

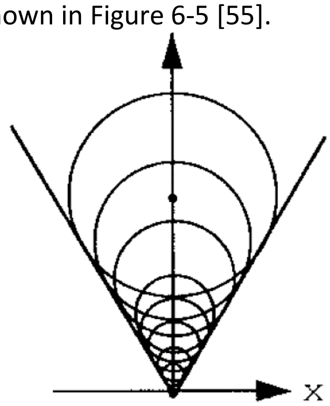

Figure 6-5: Illustration of Coma with a concentric shell telescope

As the driving specification for most NASA projects is the encircled energy [56], the end result of each of the alignment tolerance is related to its increase in the image size from the predicted value. This is done in both the spatial and the angular domain, switching between the two by simply scaling by the focal length of the system. The following analysis was originally performed by Harvey and Gresslar [55].

Examining the alignment of each primary with its respective secondary in a Wolter type-1 design, the two main considerations are the location of the mirrors along the optical axis, since the conic foci are ideally overlapping, and the tilt of each of the mirrors with respect to each other.

The impact of a misalignment along the optical axis of the secondary with respect to its ideal location is illustrated in Figure 6-6 [55]. The misalignment is characterized by Equation 6.1 [55].

$$Angular\ RMS\ Img.Dia. = \frac{\Delta \mathrm{l_{rms}}}{16f}\sqrt{\frac{1}{f^2 A_T}\sum_{n=1}^{N} D_n^2 A_n} \qquad (6.1)$$

Where there is an rms axial separation between each of the N mirror shells. The total collecting area of the telescope is A_T with each shell contributing A_n to that area with an outer diameter of D_n at that shell. Inserting the numbers for the XSPECT telescope that was launched in 1993, a 1mm axial misalignment will only contribute a 0.12 arcsec increase in the angular spot size at the focal plane. This relatively small increase in spot size for a drastic change in the axial position means that the system as a whole is not particularly sensitive to such alignment errors.

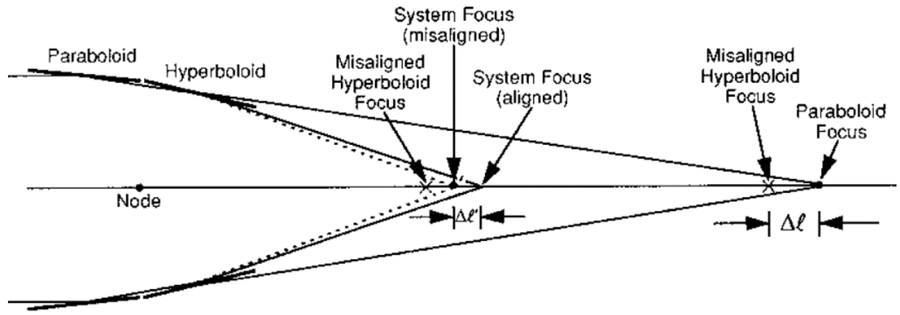

Figure 6-6: Illustration of axial misalignment in a Wolter Type-1 telescope

The angular misalignment of the secondary mirror to its respective primary mirror however, there is a much larger contribution to the angular image size. This can be described much more simply than the axial misalignment with Equation 6.2 [55].

$$Angular\ RMS\ Img.Dia. = 2\sqrt{2}\theta_{rms} \tag{6.2}$$

Again applying the number from the XSPECT telescope to this problem, the RMS error for each of the shells is 12 arcsec which means that the overall contribution to the angular spot size is ~ 40 arcsec. While the telescope is significantly more sensitive to the angular misalignments, illustrated in Figure 6-7 [55], their contributions can be cancelled by a decenter of the secondary relative to its ideal position, as it will also contribute some coma to the system.

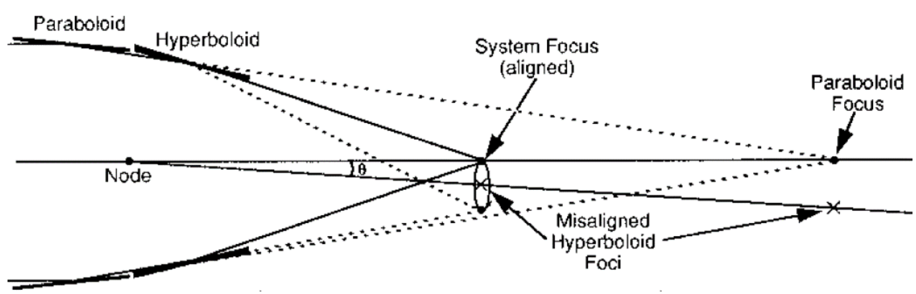

Figure 6-7: Illustration of angular misalignment in a Wolter Type-1 telescope

Finally, the alignment of each of the shell pairs to each of the other shell pairs must be considered. For this, each of the misalignments must be considered individually. This adds another term that needs to be considered as the decenter of a group of shells will create a separate image rather than generate coma that can cancel with the coma generated from the tilt offset.

Considering the extra decenter term, illustrated in Figure 6-8 [55], the increase in the angular RMS spot size is a simple extrapolation, noting that the increase in the spatial spot size will simply be by the amount of decenter.

$$Angular\ RMS\ Img.Dia. = \frac{2\delta_{rms}}{f} \tag{6.3}$$

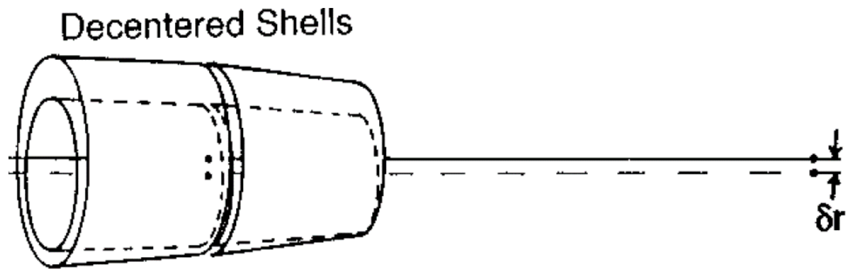

Figure 6-8: Illustration of decenter of a primary-secondary pair

The axial misalignment of a primary-secondary pair is almost exactly the same as that for just the secondary except that there is not a factor of 16 in the denominator to correct for the longitudinal magnification of the secondary mirror [55].

Finally, the angular alignment of a primary-secondary pair needs to be considered. This misalignment is illustrated in Figure 6-9 [55], and described mathematically by Equation 6.4 [55].

$$Angular\ RMS\ Img.Dia. = 2\sqrt{\frac{1}{A_T}\sum_{n=1}^{N} A_n 5(4\alpha_n\theta_n)^2} \tag{6.4}$$

Where α_n is the incident angle of a ray on the n^{th} shell.

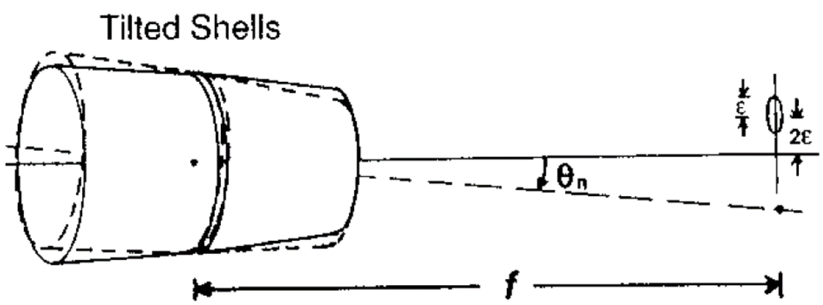

Figure 6-9: Illustration of tilt of a primary-secondary pair

6.1.4 Surface Scatter

One of the often neglected parts of the design that often dominates the end performance of the system is scattering from not atomically smooth surfaces. This becomes especially important when working with such short wavelengths, as the surface roughness generally only has an effect on the quality of the image if the deviations from the ideal smooth surface are sized on the order of the incident wavelength of light. With wavelengths that are approximately the size of the atoms that construct the reflecting surfaces even the slightest non-uniformities appear large. It is also important to realize that the RMS surface departure is not always the best indicator of the actual finish at all areas of the surface, since it is the average over the entire area. While the RMS surface departure is still the driving specification, an approximately uniform error across the surface is important as well.

As described by Harvey [57], the surface scatter based on the RMS surface roughness, $\hat{\sigma}_s$, can be represented by Equation 6.5.

$$H_s(\hat{x},\hat{y}) = \exp\left\{-(4\pi\hat{\sigma}_s)^2\left[1-\frac{\hat{C}_s\left(\frac{\hat{x}}{\hat{l}},\frac{\hat{y}}{\hat{l}}\right)}{\hat{\sigma}_s^2}\right]\right\} \tag{6.5}$$

Where $\hat{C}_s(\hat{x},\hat{y})$ is the autocovariance function of the surface. The autocovariance function is a description of the amount that the surface is varying at a given distance away from the point of interest. As would be expected, when the displacement approaches infinity, the autocovariance goes to zero and as the displacement goes to zero, the autocovariance goes to 1 and the surface scatter approaches its maximum as well. It is important to note that all of the variables in Equation 6.5 are scaled by the wavelength of light. This reiterates the point that surface irregularities are generally only a problem when they are on the same scale as the wavelength of incident light.

When performing this analysis, it is important to also look at how the transfer functions operate in the Fourier domain, as the encircled energy can be directly calculated as an integral in the Fourier domain [49]. In the Fourier domain, the overall $\hat{\sigma}_s$ for the entire surface can be thought of as a simple sum of all of the errors that are present in the system. There will be the overall surface finish, which will have very high spatial frequency content, there will be larger scale surface irregularities that will affect the scatter, which will have mid-level spatial frequency content, and finally there will be an overall error of the defined surface figure, which will have very low spatial frequency content [58]. This is all summarized in Figure 6-10 [49].

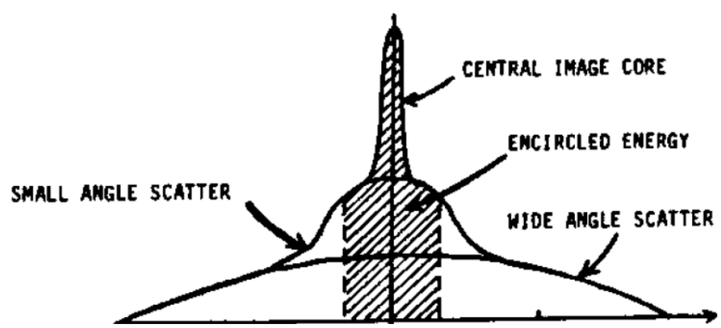

Figure 6-10: PSF of surface scatter on image intensity distribution

When all of these portions are summed together a complete picture of the transfer function of the surface comes into view. The central image core has a finite width because of the imperfections in the overall figure of the surface, where a perfect imaging surface would simply have an infinitely thin peak at the center. The small angle scatter has a direct effect on the encircled energy of the system, but as the area of integration is increased, the wide angle scatter begins to dominate. Both of these effects are only due to the imperfections in the surface finish.

It has been mentioned previously that the impact of the surface finish is reduced when used in a grazing incidence system. Mathematically, it can be represented in Equation 6.6 [58] with the addition of a scaling sine factor compared with Equation 6.5. The locations of the irregularities remains unchanged, only their impact on the final image.

$$H_r(\hat{x},\hat{y}) = \exp\left\{-(4\pi\sin(\phi)\,\hat{\sigma}_s)^2\left[1-\frac{\hat{C}_s\left(\frac{\hat{x}}{\hat{l}},\frac{\hat{y}}{\hat{l}\sin(\phi)}\right)}{\hat{\sigma}_s^2}\right]\right\} \tag{6.6}$$

Examining the impact on scattering in multilayer thin films, the picture becomes much different. Instead of examining only the amount of scatter from one surface, the contributions from every surface must be considered. There will also be a strong correlation between the errors in each surface, as shown in Figure 6-11 [59], although there will also be errors that will be localized to a single layer of the thin film. These localized errors will have the highest spatial frequency, where the errors that are replicated at each layer will have the mid-level spatial frequencies. While the overall figure error will also be replicated on each layer, its impact on the scattering is much lower than for the mid-spatial frequencies.

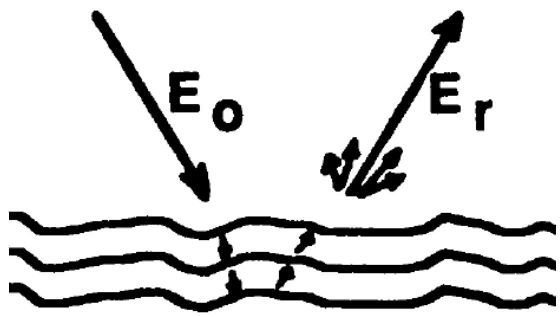

Figure 6-11: Scattering effects from a multilayer

The general analysis of the system is very similar, although the compounded effects from each surface end up causing the mid-spatial frequency variations to have a much larger effect on the image performance, as shown in Figure 6-12 [59], compared with Figure 6-10.

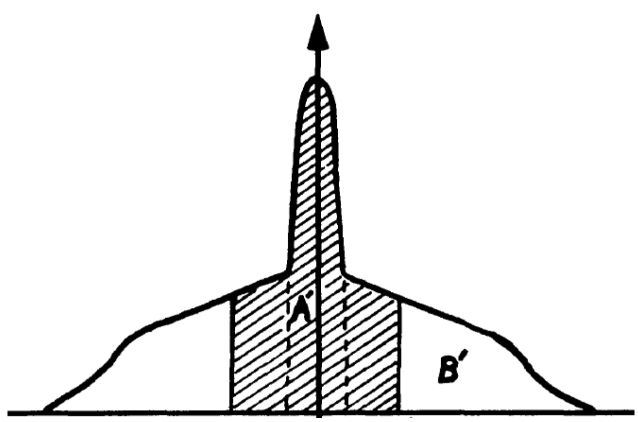

Figure 6-12: PSF of multilayer scatter on image intensity distribution

When simulations of these surface errors are performed, it is also very clear that the effects of multilayer scatter are dominated by the mid-spatial frequency components that are replicated on each surface and have the largest effect on imaging performance [60].

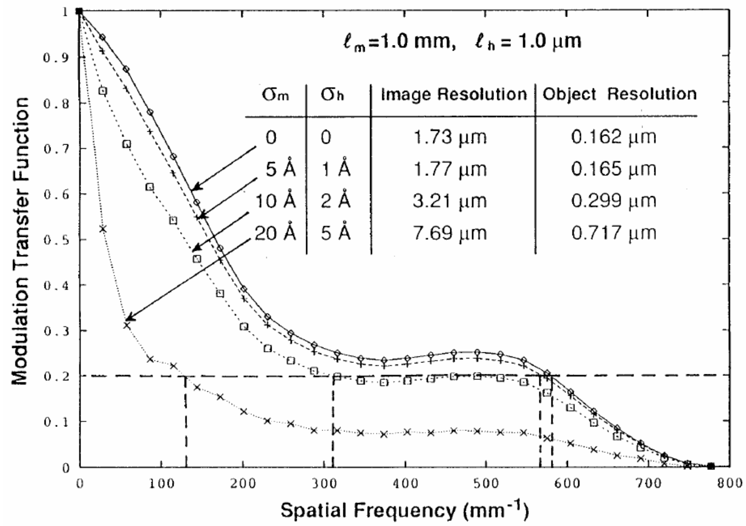

Figure 6-13: Multilayer scattering impacts on MTF perfrmance

6.2 Refracting Systems

The manufacturing of the CRL assemblies creates more of a design challenge than does their use. The materials that work best for CRLs, those that have very high index decrements but also very low absorption such as Lithium [43], are not necessarily safe to handle in a regular lab environment. Special safety precautions need to be taken when working with materials such as Lithium. That being said, there are many different ways in which a metal can be manufactured to create the necessary shapes for a CRL assembly.

Perhaps the most precise method that can be used to make the lenses is to mill or press the lenses individually. While this takes the most amount of time, there is complete control of each of the individual lenses. Care must be taken that there is a precise alignment in the location of the lens within the housing, as the CRL must have near perfect alignment for each lens in order to function properly. Figure 6-14 [61] shows a parabolic indenter that can be used to press the shape of the lenses into a soft metal such as Lithium [61].

Another method that is less costly in terms of both time and money is extrusion. This method allows for an entire grouping of lenses to be manufactured simultaneously. If hot extrusion is used, then there is also good uniformity for each of the lenses. This is different from pressing or milling where each lens is made individually and errors could be specific to a single lens. This method does not provide for as much control over the system however, even though the die that is used for the extrusion is made to a very high degree of accuracy. The automation of this process is what makes it much more appealing.

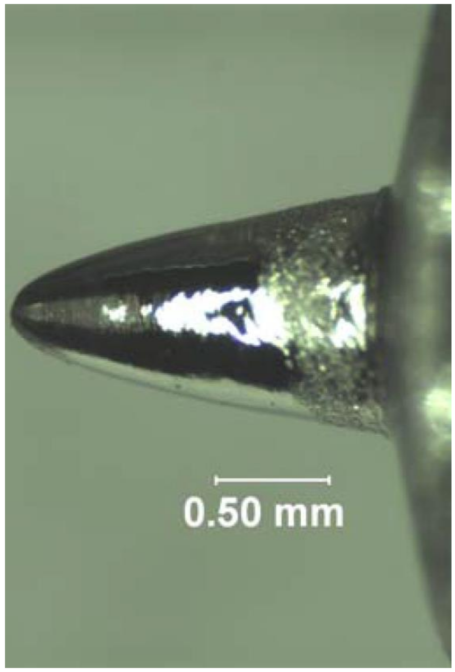

Figure 6-14: Indenter used to press CRLs

6.3 Diffraction Systems

For most diffraction optics, there is a much greater difficulty in manufacturing than in most optics designs, because of the exact wavelength dependent nature of diffraction, all of the tolerances need to be on the order of wavelengths for accuracy. For x-ray optics, since all of the manufacturing techniques require wavelength level accuracy, the challenge is not much greater than other techniques, which actually makes it a valuable tool without the typical increase in effort that is required.

For diffraction gratings, the manufacturing techniques are very similar to those for visible optics, because the grating lines are spaced at similar distances since it is the grazing incidence angle that reduces the effective spacing, making them useful for x-rays. There are a few different techniques that have been used to create reflective gratings. One of those techniques that is comparable to manufacturing the individual lenses of a CRL is to mill out each of the individual grooves of a grating [44]. This process, while very controlled, comes with many drawbacks, mainly that the cutting tool will never be able to create a perfectly sharp edge as the theory describes, and often the tools will chip away pieces of the substrate during this process. This is one of the oldest techniques however and is relatively simple, but very time consuming.

Lithography is a method that has become much more popular recently to manufacture many different types of diffraction optics. Lithography can easily be used to create sinusoidal rather than square diffractive gratings by using plane wave interference [44]. These plane waves will create evenly space interference fringes, that when exposed to a photosensitive material, will imprint their pattern. A common set-up for this is using Lloyd's Mirror in which the film will be place perpendicular to a mirror, and that mirror will be tilted with respect to the incident plane wave. The generated interference pattern will be perpendicular to the film and the pattern will be imprinted.

There have been several different manufacturing techniques that have evolved over the last several years that have led to great advances in the use of Fresnel zone plates in x-ray imaging. Amplitude zone plates for visible optics are typically manufactured by first creating a glass blank and then depositing an opaque thin film onto that surface which will act as an amplitude diffraction grating. This technique is difficult to replicate in the x-ray regime for several reasons, primarily because the absorption of most materials is very large, preventing most of the light from actually making it to the focus of the zone plate. A creative method of manufacturing has been used in recent years that has made zone plates a more viable option for x-rays and that is the sputtered-slice technique. In this technique, a wire, typically made of Au, is coated with another material that is much more opaque to x-rays. That opaque layer is then coated with gold and the process is repeated to create as many layers on the wire as there will be zones in the zone plate. This sputter coated wire is then sliced to the desired thickness that will create the desired level of contrast between the transmitted x-rays in each zone. This process is illustrated in Figure 6-15 [62] for a Cu-Al zone plate..

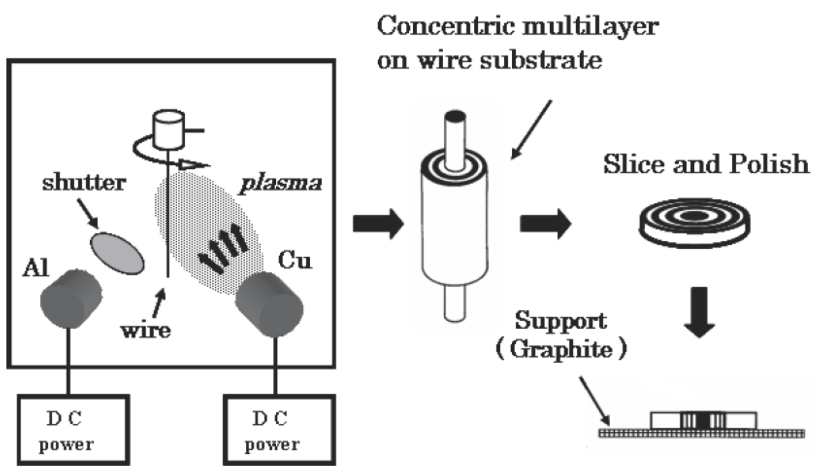

Figure 6-15: Manufacturing process of Sputtered-sliced Fresnel Zone plates

The sputtered-sliced technique has become much more popular in recent years because it is much easier to manufacture than simply depositing layers on a glass blank and is also much more reliable and quick. It has also been shown that this technique can create zone plates that are capable of imaging objects that are $< 0.1\mu m$ in size [63].

For the phase modifying zone plates, there are a few different methods in which the manufacturing has moved forward. Initially, the method for manufacturing was almost exclusively a lithographic technique in which a glass blank was first completely covered with a coating that was as thick as the thickest section needed to be. Then, each of the layers was etched away until they were the necessary thickness. This technique, illustrated in Figure 6-16 [46], is still used today, although there are other methods that have become slightly more favorable in recent years with the increase in thin film deposition technology.

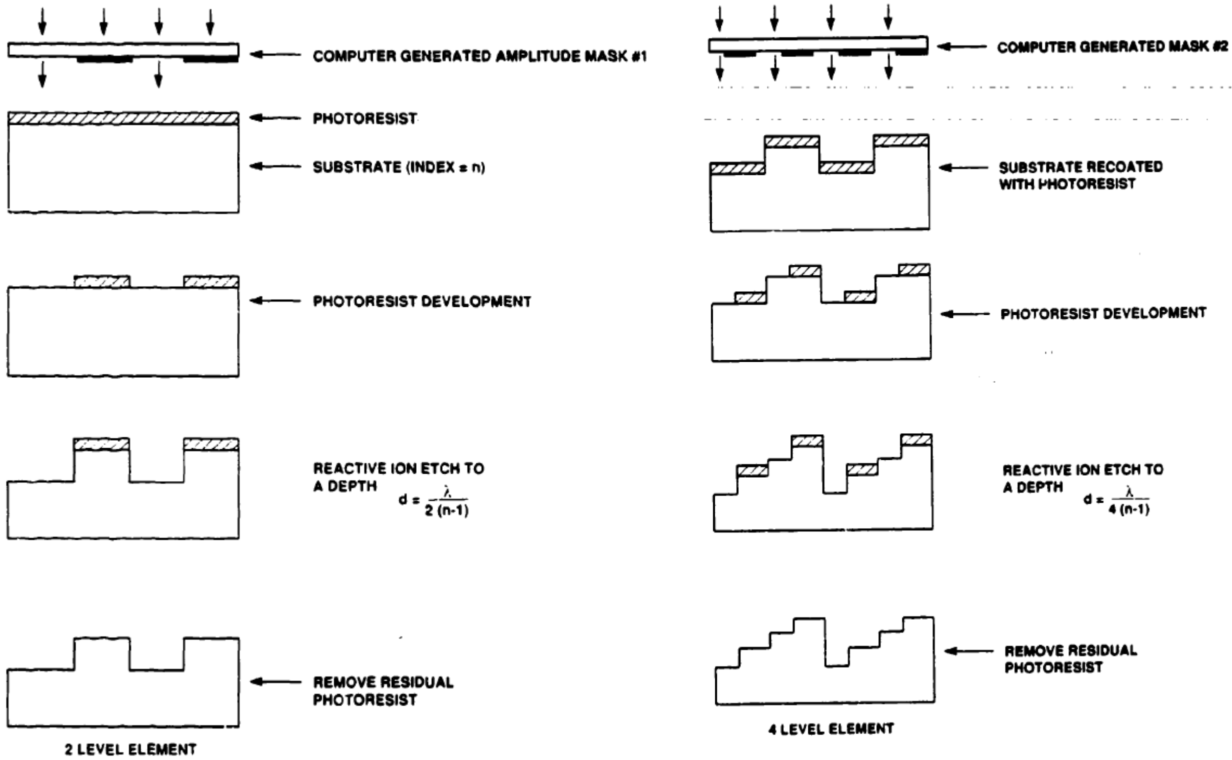

Figure 6-16: Etching process for the manufacture of multi-layer Fresnel zone plates

The newer techniques have found a middle ground between the amplitude and the multilayer zone plates. These newer methods still only use the two materials that are used in the sputtered-sliced technique, but create composite materials that combine to make an effectively new material that will provide the same phase change after transmission as a layer that is made of the denser material but half as thick. This concept is best shown in Figure 6-17b and Figure 6-17e which are functionally equivalent [62]. The same is true for Figure 6-17f and Figure 6-17c. By creating a composite layer that has an index decrement that is half of that of the thickest layer, the same OPD is created as having half of that higher index layer. One of the major benefits here is that the same chamber can be used for the entire process, only controlling the deposition rates of the materials, rather than needed to precisely apply the photoresist multiple times over the course of the manufacturing.

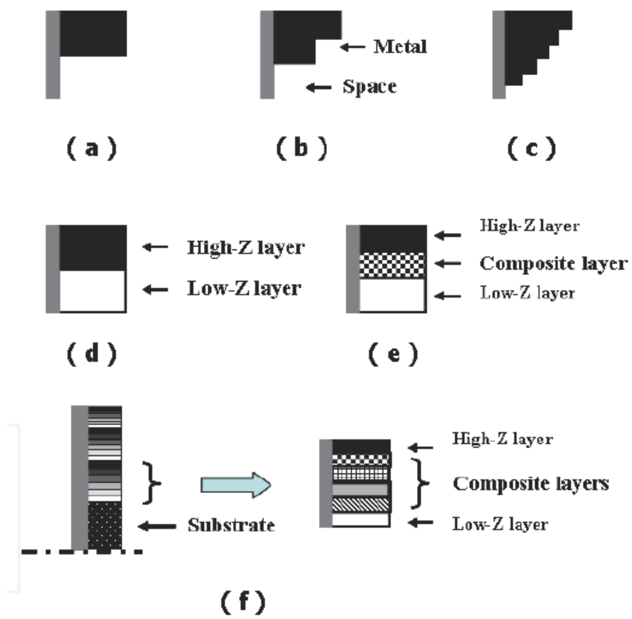

Figure 6-17:Composite layers and their equivalent multilayer diffraction components

7 References

[1] W. Roentgen, "On a New Kind of Rays," *Nature,* vol. 53, pp. 274-277, 1896.

[2] E. Spiller, "2. Optical Constants," in *Soft X-Ray Optics*, Bellingham, Washington, SPIE, 1994, pp. 5-22.

[3] A. G. Michette, "1. Properties of Soft X-Rays," in *Optical Systems for Soft X-Rays*, New York, New York, Plenum Press, 1986, pp. 1-36.

[4] H. A. Lorentz, The Theory of Electrons and its Applications to the Phenomena of Light and Radiant Heat, New York, New York: G. E. Stechert and Co., 1916.

[5] L. B. N. Laboratory, X-Ray Data Booklet, Berkeley, CA, 2001.

[6] Tiger66, "Wikimedia Commons," 31 December 2012. [Online]. Available: https://commons.wikimedia.org/wiki/File:HuygensWavePropagation.svg. [Accessed February 2016].

[7] jkrieger, "Wikimedia Commons," 16 March 2012. [Online]. Available: https://commons.wikimedia.org/wiki/File:Single_Slit_Diffraction.svg. [Accessed Feb 2016].

[8] A. G. Michette, "4. Reflective Optics for Soft X-Rays II. Multilayer Mirrors," in *Optical Systems for Soft X-Rays*, New York, New York, Plenum Press, 1986, pp. 95-110.

[9] T. Takahashi, "The ASTRO-H X-ray Observatory," *SPIE Space Telescopes and Instrumentation: Ultraviolet to Gamma Ray,* vol. 8443, 2012.

[10] P. Kirkpatrick and A. Baez, "Formation of Optical Images by X-Rays," *OSA,* vol. 33, no. 9, pp. 766-774, 1948.

[11] R. Hudec, "Kirkpatrick-Baez (KB) and Lobster Eye (LE) Optics for Astronomical and Laboratory Applications," *X-Ray Optics and Instrumentation,* vol. 2010, no. 139148, 2010.

[12] M. Montel, "The X-Ray Microscope with Catamegonic Roof Shaped Objective," in *Proceedings fo a Symposium Held at the Cavendish Laboratory*, Cambridge, Massachusetts , 1956.

[13] W. Liu, "Achromatic Nested Kirkpatrick-Baez Mirror Optics for Hard X-ray Nanofocusing," *Journal of Synchrotron Radiation,* vol. 18, pp. 575-579, 2011.

[14] G. Resta, B. Khaykovich and D. Moncton, "Nested Kirkpatrick-Baez (Montel) Optics for Hard X-Rays," *Journal of Applied Crystallography,* vol. 48, no. 2, pp. 558-564, 2015.

[15] S. Matsuyama, "Diffraction-limited two-dimensional hard-x-ray focusing at the 100nm level using a Kirkpatrick-Baez mirror arrangement," *Review of Scientific Instruments,* vol. 76, 2005.

[16] P. Friedrich, "Wolter Optics," in *The Universe in X-Rays*, New York, New York, Springer, 2008, pp. 41-50.

[17] J. E. Harvey, "Diffraction Effects in Grazing Incidence X-Ray Telescopes," *Journal of X-Ray Science and Technology,* vol. 3, pp. 68-76, 1991.

[18] "Conical Foil X-Ray Telescope Performance Predictions for Space Astronomy Applications," *SPIE Multilayer and Grazing Incidence X-Ray/EUV Optics II,* vol. 2011, pp. 182-192, 1993.

[19] A. Last, "X-Ray Optics," January 2008. [Online]. Available: http://www.x-ray-optics.de/. [Accessed November 2015].

[20] P. Thompson, "Optical Performance of Grazing Incidence X-Ray/EUV Telescopes for Space Science Applications," School of Optics at the Univeristy of Central Florida, Orlando, Florida, 2000.

[21] A. Kotha and J. E. Harvey, "Enhanced EUV Performance of Wolter Type II Telescopes," *SPIE Multilayer and Grazing Incidence X-Ray/EUV Optics II,* vol. 2011, pp. 34-46, 1993.

[22] T. T. Saha, "General Surface Equations for Glancing Incidence Telescopes," *Applied Optics,* vol. 64, no. 4, pp. 658-663, 1987.

[23] T. T. Saha, "A generalized sine condition and performance comparison of Wolter type II and Wolter-Schwarzschild Extreme Ultraviolet Telescopes," *SPIE Advanced Technology Optical Telescopes II,* vol. 0444, pp. 112-117, 1983.

[24] P. L. Thompson and J. E. Harvey, "Systems engineering analysis of aplanatic Wolter Type-1 X-Ray Telescopes," *SPIE Optical Engineering,* vol. 39, no. 6, pp. 1677-1691, 2000.

[25] J. E. Harvey, A. Krywonos, P. L. Thompson and T. T. Saha, "Grazing-Incidence Hyperboloid-Hyperboloid Designs for Wide-Field X-ray Imaging Applications," *Applied Optics,* vol. 40, no. 1, pp. 136-144, 2001.

[26] D. Korsch, "Imaging analysis of mirrors from normal to grazing incidence," *OSA,* vol. 66, no. 9, pp. 938-941, 1976.

[27] C. E. Winkler and D. Korsch, "Primary Aberrations for Grazing Incidence," *Applied Optics,* vol. 16, no. 9, pp. 2464-2469, 1977.

[28] T. T. Saha, "Aberrations for Grazing Incidence Telescopes," *Applied Optics,* vol. 27, no. 8, pp. 1492-1498, 1988.

[29] W. K. H. Schmidt, "A Proposed X-Ray Focusing Device with Wide Field of View for use in X-Ray Astronomy," *Nuclear Instruments and Methods,* vol. 127, no. 2, pp. 285-292, 1975.

[30] J. R. P. Angel, "Lobster Eyes as X-Ray Telescopes," *SPIE Space Optics - Imaging X-Ray Optics Workshop,* vol. 184, pp. 84-85, 1979.

[31] L. Sveda, R. Hudec, L. Pina, V. Semencova and A. Inneman, "Lobster eye: technology and imaging properties," *SPIE EUV and X-Ray Optics: Synergy between Laboratory and Space,* vol. 7360, 2009.

[32] W. Zhang, A. G. Peele, R. Petre, Y. Soong and N. E. White, "A Practical Implementation of the Lobster Eye Optics," in *SPIE Conference on X-Ray Optics, Instruments, and Missions*, San Diego, CA, 1998.

[33] R. Hudec, L. Pina and A. lnneman, "Replicated Grazing Incidence X-Ray Optics: Past, Present andFuture," in *SPIE Conterence on X-Ray Optics, Instruments, and Missions II*, Denver, CO, 1999.

[34] A. Inneman, R. Hudec and L. Pína, "Progress in Lobster - Eye X-ray optics development," *SPIE X-Ray Optics, Instruments, and Missions IV,* vol. 4138, pp. 94-104, 2000.

[35] E. Spiller, "8. Design of Multilayer Structures," in *Soft X-Ray Optics*, Bellingham, Washington, SPIE, 1994, pp. 139-168.

[36] E. Spiller, "Low-Loss Reflection Coatings using Absorbing Materials," *Applied Physics Letters,* vol. 20, no. 9, pp. 365-367, 1972.

[37] E. Spiller, "Reflective multilayer coatings for the far uv region," *Applied Optics,* vol. 15, no. 10, pp. 2333-2338, 1976.

[38] R. T. Perkins, J. M.Thorne and H. K. Pew, "Theoretical Considerations in the Design of Multilayer X-Ray Optics," *SPIE X-Ray Imaging II,* vol. 691, pp. 76-82, 1986.

[39] E. Spiller and A. E. Rosenbluth, "Determination of thickness errors and boundary roughness from the measured performance of a multilayer coating," *SPIE Applications of Thin-Film Multilayered Structures to Figured X-Ray Optics,* vol. 563, pp. 222-236, 1985.

[40] R. B. Hoover, D. L. SHealy and S.-H. Chao, "Spectral Slicing X -Ray Telescope," *SPIE Optical Engineering,* vol. 25, no. 8, pp. 970-978, 1986.

[41] I. A. Artioukov and K. M. Krymski, "Schwarzschild objective for soft x-rays," *SPIE Optical Engineering,* vol. 39, no. 8, pp. 2163-2170, 2000.

[42] I. A. A. e. al, "Reflective soft x-ray microscope for the investigation of objects illuminated by laser-plasma radiation," *Quantem Electronics,* vol. 25, no. 9, pp. 919-922, 1995.

[43] K. Young and A. Khounsary, "Extrusion of Compound Refractive X-ray Lenses," in *Design and Microfabrication of Novel X-Ray Optics II*, Denver, CO, 2004.

[44] A. G. Michette, "7. The Design and Manufacture of X-Ray Diffraction Gratings," in *Optical Systems for Soft X-Rays*, New York, New York, Plenum Press, 1986, pp. 147-163.

[45] E. Spiller, "6. Zone Plates," in *Soft X-Ray Optics*, Bellingham, Washington, SPIE, 1994, pp. 81-99.

[46] G. J. Swanson, "Binary Optics Technology: The Theory and Design of Mulit-level Diffractive Optical Elements," Lincoln Laboratory, Massachusetts Institute of Technology, 1989.

[47] A. G. Michette, "8. Diffractive Optics II: Zone Plates," in *Optical Systems for Soft X-rays*, New York, New York, Plenum Press, 1986, pp. 165-216.

[48] P. B. Reid, "X-Ray Telescopes," in *Encyclopedia of Astronomy and Astrophysics*, Basingstoke, Hamphsire, United Kingdom, Nature Publishing Group, 2001.

[49] J. E. Harvey, E. C. Moran and W. P. Zmek, "Transfer function characterization of grazing incidence optical systems," *Applied Optics,* vol. 27, no. 8, pp. 1527-1533, 1988.

[50] A. Slomba, R. Babish and P. Glenn, "Mirror Surface Metrology and Polishing for AXAF/TMA," *SPIE X-Ray Instrumentation in Astronomy,* vol. 597, pp. 40-54, 1985.

[51] F. A. Harrison, "The Nuclear Spectroscopic Telescope Array (NuSTAR) High-Energy X-ray Mission," *The Astorphyical Journal,* vol. 770, no. 103, 2013.

[52] C. Falco, *Course Notes for OPTI 576 at Univeristy of Arizona,* Tucson, AZ, 2014.

[53] C. Falco, "Multilayer Soft X-Ray Optics," in *Fifty Years of Optical Sciences at The University of Arizona*, San Diego, California, 2014.

[54] A. E. Rosenbluth, "Computer Search for Layer Materials that Maximize the Reflectivity of X-Ray Multilayers," *Revue de Physique Appliquee,* vol. 23, pp. 1599-1621, 1988.

[55] J. E. Harvey and W. J. Gresslar, "Image Degradation due to Assembly and Alignment Errors in Conical Foil X-Ray Telescopes," *SPIE Optical Engineering,* vol. 35, no. 10, pp. 3037-3047, 1996.

[56] J. E. Harvey, Interviewee, [Interview]. 11 2015.

[57] J. E. Harvey, K. L. Lewotsky and A. Kotha, "Effects of surface scatter on the optical performance of x-ray synchrotron beam-line mirrors," *Applied Optics,* vol. 34, no. 16, pp. 3024-3032, 1995.

[58] J. E. Harvey, "Chapter 11 X-Ray Optics," in *Handbook of Optics, 2nd Ed*, McGraw Hill, 1995.

[59] J. E. Harvey, W. P. Zmek and C. Ftaclas, "Imaging Capabilities of Normal Incidence X-Ray Telescopes," *SPIE Optical Engineering,* vol. 29, no. 6, pp. 603-608, 1990.

[60] J. E. Harvey, K. L. Lewotsky and A. Kotha, "Performance predictions of a Schwarzschild imaging microscop for soft x-ray applications," *SPIE Optical Engineering,* vol. 35, no. 8, pp. 2423-2436, 1996.

[61] A. Khounsarya, E. M. Dufresne, K. Young, C. M. Kewish and A. N. Jansen, "Beryllium and lithium X-ray lenses at the APS," in *Advances in X-Ray/EUV Optics, Components, and Applications*, San Diego, CA, 2006.

[62] S. Tamura, "Multilayer Fresnel Zone Plate with High-Diffraction Efficiency: Application of Composite Layer to X-ray Optics," in *Metal, Ceramic and Polymeric Composites for Various Uses*, Rijeka, Croatia, Intech, 2011.

[63] N. Kamijo, "Characterization of Sputtered-sliced Fresnel Zone Plate at BL20XU: High-Resolution Hard X-Rya Microbeam Experiments," *Instrumentation and Methodology,* pp. 111-113.

[64] A. G. Michette, "3. Manufacture of Grazing Incidence Reflective Optics," in *Optical Systems for Soft X-Rays* , New York, New York, Plenum Press, 1986, pp. 67-94.

[65] A. G. Michette, "9. Manufacture of Zone Plates," in *Optical Systems for Soft X-Rays*, New York, New York, Plenum Press, 1986, pp. 217-241.